LUND UNIVERSITY

Measuring ammonia

Development and application of measurement techniques for the detection of ammonia

Odd Magnar Hole

Master thesis in Physics (60 ECTS)
University of Lund
In cooperation with the department for Combustion Physics in Lund and Scania
Spring/Autumn 2012

Supervisor: Zhongshan Li

Measuring ammonia – Development and application of measurement techniques for the detection of ammonia

Master thesis in Physics – February, 2013

Lund Report on Combustion Physics, LRCP-165
ISRN LUTFD2/TFC – 165 – SE
ISSN 1102-8718

Odd Magnar Hole

Division of Combustion Physics,
Department of Physics
Lund University

P.O. Box 118
S-221 00 Lund
Sweden

Abstract

Ammonia (NH_3) is an important chemical both as a chemical precursor and in its own right. It is therefore of practical importance to be able to visualize ammonia gas especially when ammonia is present in combustion or flue-gas environments. This thesis is focused on the use of laser-induced fluorescence with the stated aim of imaging ammonia in low concentrations, with the end-goal of applying the technique to evaluate the flow of ammonia into, and out from, a NOx-reduction catalysis unit. The fluorescence was induced using a two-photon excitation scheme using a laser with an output wavelength of 305 nm and detection of the fluorescence at 555-575 nm. In order to accurately evaluate the signal, extensive testing of the parameters influencing the signal was carried out. Dependencies of temperature, pressure, concentration, stimulated emission and laser power was evaluated experimentally.

Using the data from the temperature measurements, a simulated spectrum of the probed transition was fitted, enabling the relevant molecular constants to be extracted. At low irradiances, corresponding to the “linear” regime of regular one-photon LIF, the signal shows a quadratic dependence on laser power. Stimulated emission, or amplified spontaneous emission, show a fifth order dependence on laser irradiance, but this emission was not measurable at the levels of irradiance used for imaging. With a constant concentration, the signal increases slightly with pressure up to 2 bar and the decrease due to collisional quenching. The signal shows a linear dependence on concentration within the evaluated concentration region. The detection limit with the setup used is estimated at 800 ppm, and single-point measurements could potentially measure sub-ppm concentrations.

The technique was successfully implemented for the imaging of laminar and turbulent flames, as well as imaging of the gas immediately above a small sample of ammonia-reducing catylic material.

Populärvetenskaplig sammanfattning

Spektroskopins historia började med Isaac Newtons optiska experiment i perioden 1666–1672. Newton använde ordet ”spektrum” för att beskriva den regnbåge av färger som blir synlig när vitt ljus passerar genom ett prisma. Newton insåg att det vi upplever som vitt ljus egentligen är en kombination av alla färgarna i detta spektrum. Blickar vi framåt i tiden, till 1800-talet, kan vi se att Joseph von Fraunhofer genomförde experiment med diffraktionsgitter istället för prismor. Ett gitter ger mycket större spridning av färgerna och därmed ökar möjligheten att se mindre detaljer i spektra. Med denna nya teknik kunde von Fraunhofer observera att det finns tunna linjer i regnbågsspektra från solen där färgen tycktes vara borta. Sedan upptäcktes det att upphettade molekyler och atomer skickade ut ljus som lyste upp i tunna linjer i ett spektrum. Dessa tunna ljuslinjer visade sig att vara de samma ljuslinjer som molekyler och atomer tog bort från vitt ljus. Två pusselbitar passade nu ihop; linjerna som fattades från solspektra hade blivit absorberade av de molekyler och atomer som finns mellan solen och våra instrument, i jordens och solens atmosfär.

Idag har vi mer sofistikerade verktyg när vi analyserar ljus, men grundprinciperna är fortfarande de samma som i spektroskopins barndom. Ett mycket viktigt nytt verktyg är lasern. En laser kan åstadkomma ljus med mycket hög intensitet där ljuset ger en smal linje av färg i dess spektrum. Med mer moderna teorier kan detta förklaras som att laserljusets fotoner alla har praktiskt taget samma energi eller våglängd. Med en laser kan man då skicka ljus genom en gas, där ljusets energi är sådan att det endast kan absorberas av en enstaka typ av molekyler. Detta kan användas som en mätmetod på ett direkt sätt, genom att mäta intensiteten på det laserljus som lyckas komma genom gasen kan densiteten av de molekyler som absorberar ljuset beräknas.

I denna uppsats används laserljuset på ett annat sätt; en molekyl som absorberar energi i form av en ljusfoton blir exciterad och hamnar i ett högre energitillstånd. En grundregel i naturen är att alla system förr eller senare hamnar i sitt lägsta energitillstånd; molekylen kommer således att

behöva göra sig av med sin absorberade energi. Den extra energin kan avlägsnas genom flera olika processer, men i denna uppsats kommer det fokuseras på emission. Vid emission skickar den exciterade molekylen ut en foton vars energi motsvarar energiskillnaden på det exciterade energitillståndet och det tillstånd molekylen övergår till. Den utskickade fotonen kan detekteras och det är då möjligt att observera var molekylen befann sig då den emitterade fotonen. Med en känslig kamera kan man filma laserstrålen från sidan och på så sätt visualisera var i laserstrålen en viss molekyl befinner sig. Detta är ett mycket värdefullt verktyg om man till exempel behöver titta på hur molekyler rör sig i ett gasflöde, en flamma, ett rörsystem eller i en förbränningskammare. Man kan också använda tekniken till att titta på kortlivade molekyler som uppstår som mellanled i reaktioner, till exempel i en förbränningsprocess. Denna teknik kallas ”laserinducerad fluorescens” (LIF).

Då större flödesstrukturer behöver iakttas kan ett “ark” av laserljus konstrueras med hjälp av linser. En laser ger oftast ljus i ett smalt strålknippe, en mycket stark ”prick” av ljus. Med linser kan man sträcka ut denna prick i en riktning och smalna av den i en annan, och på så sätt ändra laserprofilens form från en liten cirkel till ett smalt streck. Sett från sidan blir detta smala streck ett ”ark” eller plan av laserljus. Alla molekyler som exciteras av laserljuset kommer nu ha bestämda avstånd till kameran; de kommer alla vara inom det tunna planet av laserljus.

I arbetet bakom denna uppsats har LIF använts för att studera ammoniak. Ammoniak är en mycket viktig molekyl som används inom industrin men också som en del av livscykeln för landlevande organismer. I samarbete med Scania CV AB (NOx Treatment System) var målet att utvärdera möjligheterna att använda LIF-tekniken för att förbättra katalyseringen av NOx-gaser som bildas i dieselmotorer. Ammoniak ingår i katalysprocessen som en viktig reaktant som gör reduceringen av NOx-gaser möjlig. Uppsatsens slutsats är att mätningar och visualisering av ammoniak är möjligt med LIF. Gränsvärden och viktiga parametrar har uppmätts; problemområden och möjligheter för förbättring har identifierats. Mätmetoden har använts till att titta på turbulenta flammor samt ammoniakkoncentrationen över en yta av katalysmaterial.

Table of contents

1 Introduction

1.1 Background

Imaging techniques using lasers have many advantages when compared to conventional techniques. Firstly, the laser techniques do not disrupt the local measurement environment. A physical probe can influence the flow, temperature and even chemical composition of its immediate surroundings; whereas laser probes seldom interact in a disruptive manner. Secondly, laser techniques have superior temporal and spatial resolution. The short pulses of the laser make it possible to image even in turbulent conditions. The high spatial resolution enables evaluation of sharp gradients within the measured volume. Thirdly, laser techniques can be applied even in extreme conditions. As the measuring equipment is not in physical contact with the measurement environment, effects of corrosion, rapid flow, extreme temperatures and pressures do not damage the measuring equipment.

Ammonia is an important chemical component in industry and agriculture. It is used as a precursor for other compounds, commercially available in aqueous solutions and as an additive. The chemical properties of ammonia have in recent years become more important as the compound has found its use as an additive for NOx-reduction in flue gases. Many DeNOx processes utilize the addition of ammonia to the exhaust gas to make the NOx-reduction more efficient. It is therefore relevant to measure ammonia when evaluating such processes. To optimize a selective catalytic reduction (SCR) system it is important to determine how the ammonia interacts with the catalyst.

1.2 Aim

During the work with this thesis, methods for imaging ammonia using laser-induced fluorescence (LIF) were investigated. The goal was to determine the viability of using imaging techniques to evaluate the gas composition close to the surface of a DeNOx catalyst. Specifically, the end-goal of the project was to measure the distribution of ammonia and NO entering and exiting a catalyst plug in an exhaust system in cooperation with Scania. As no complete and tested method for imaging ammonia existed this had to be investigated and developed as a first step. This thesis will detail the development and application of this method.

2 Ammonia

Ammonia is an important chemical compound both for industrial use and life. It is a source of free nitrogen and is an integral part of the nitrogen cycle of life, and the urea cycle of mammals. In its gas form ammonia is colorless, but has a very strong and distinct smell that most people would instantly recognize.

2.1 Safety

Gaseous ammonia is a health risk at elevated concentrations, but the human body is adept at quickly neutralizing any ammonia that enters the blood stream. Exposure to low concentrations of ammonia over extended periods of time is therefore not as dangerous as would be expected from the reactive nature of the molecule. Exposures should, however, be kept at a minimum regardless. Industrial working guidelines for ammonia exposure set limits at 15 minutes for 35 ppm volume concentration in air and 8 hours for 25 ppm volume concentration. Below these levels no long-term health issues are expected. 300-600 ppm for 30-60 minutes is considered the maximum short time exposure tolerance. Exceeding this is likely to result in irreversible health issues. Exposures

of 5,000-10,000 ppm are reported to be immediately fatal. Lung damage is the most common adverse health effect of ammonia exposure.

The odor threshold of ammonia is at around 5 ppm, and so smelling ammonia can act as an early warning for a potentially dangerous buildup of ambient ammonia. Identifying leakages is also simplified by the strong smell. Adequate ventilation is needed when working with ammonia. If a person is exposed to ammonia through inhalation, move the person to fresh air and provide oxygen if breathing is difficult or artificial respiration if not breathing.

Ammonia in solution is basic and considered highly toxic to water-living organisms. The level of toxicity is much lower for humans and other mammals as bodily functions are in place to specifically hinder the buildup of ammonia in the bloodstream. In any case; leakages to the environment should be avoided [1-3].

2.2 Band structure

In its ground state the ammonia molecule has a pyramidal structure and is classed as a symmetric top [4]. The excited states show planar equilibrium configurations and four progressions from electronic transitions have been identified [5]. The first excited state of ammonia, the *A* state, is strongly predissociative and is thus not a good candidate for LIF measurements. This transition has absorption bands in the range 170-215 nm and is thus within the range of achievable laser wavelengths.

The second and third excited states, the *B* and *C* states, have absorption bands in the range 140-167.5 nm. A fourth electronic excited state, the *C'* state, was identified in the late 1970s. Emissions from transitions between the *C'* state and the *A* state of ammonia, dubbed "Schuster bands" [6, 7] had been observed previously, but was then attributed to the ammonium radical NH_4. This state is at about the same energy level as the *C* state, but the transition *X*-*C'* is forbidden due to parity, explaining why this transition was not initially attributed to ammonia; only multi-photon excitation can reach the excited *C'* state. The *X*-*C'* transition would thus not be revealed by conventional VUV absorption spectroscopy.

2.3 Selective Catylic Reduction

Ammonia is a crucial additive in the SCR process for reducing NOx in exhaust gas. For diesel engines the NOx content is dominated by NO and thus the main reduction channel is:

$$4NH_3 + 4NO + O_2 \rightarrow 4N_2 + 6H_2O$$

The intermediate steps and the kinematics of this reaction differ slightly between catylic materials. It has been found that the reaction rate when the amounts of NO and NO_2 are similar is much faster than with NO alone [8]:

$$4NH_3 + 2NO + 2NO_2 \rightarrow 4N_2 + 6H_2O$$

Because of this faster process some SCR systems include pre-catalysts to oxidize the NO in order to bring the NO/NO_2 ratio closer to one.

The SCR process is efficient only in a bounded temperature region, most often between 200-450°C. At lower temperatures the reaction rates are too slow to achieve a noticeable effect on the NOx content, and at higher temperatures reactions that produce N_2O or NO start to dominate. The reactions involved are:

$$4NH_3 + 4NO + 3O_2 \rightarrow 4N_2O + 6H_2O$$

$$4NH_3 + 5O_2 \rightarrow 4NO + 6H_2O$$

Mobile units using the SCR system usually use urea as the carrier for ammonia due to the ease of handling. Urea decomposes in the following reactions:

$$(NH_2)_2CO \rightarrow NH_3 + HNCO$$

$$HNCO + H_2O \rightarrow NH_3 + CO_2$$

It has also been found that urea can react directly with the NOx-species in the following reactions [8, 9]:

$$2(NH_2)_2CO + 6NO \rightarrow 5N_2 + 4H_2O + 2CO_2$$

$$4HNCO + 6NO \rightarrow 5N_2 + 2H_2O + 4CO_2$$

$$(NH_2)_2CO + NO + NO_2 \rightarrow 2N_2 + 2H_2O + CO_2$$

The decomposition of urea and the reduction reaction between urea and NOx can be sped up by using a urea catalyst downstream of the pre-catalyst, but before the SCR catalyst. To reduce slippage of excess ammonia, an oxidizing catalyst can be used downstream of the SCR catalyst.

3 Laser-induced Fluorescence (LIF)

The main part of this thesis was determining characteristics of the *X-C'* transition and its accompanying fluorescence signal of importance to evaluate measurements using LIF.

3.1 Principle

Laser-induced fluorescence, or LIF, is a species-specific, laser-based diagnostics tool used most notably in imaging reaction and flow features. The theoretical basis of the technique is rather simple in principle, but the interpretation of the results can be complex and difficult, especially in quantitative studies.

The basic mechanism behind the technique is to selectively excite the molecules to be measured using a suitable laser frequency. This frequency needs to be such that it fits the energy gap between two energy levels of the molecule and, ideally, the frequency should not be absorbed by other species present in the measurement volume. Following the excitation, the molecule subsequently de-excites and release photons. The emitted photons are generally distributed spectrally broader compared to the laser photons. This is because the emission transitions often involve energy levels other than the absorption transitions. Often these transitions give a lower frequency of the emitted light and are then termed “Stokes shifted”[10].

In order to extract spatial information a detector is normally placed perpendicularly to the laser beam. This detector needs to be sensitive to the frequencies emitted from the excited molecules. As the laser beam is highly coherent and directional, and the photons are isotropically emitted from the deexcitation, the only photons to reach the detector are, again ideally, the ones released from the deexcitation. In real measurements the laser photons can scatter on molecules (Rayleigh scattering) and particles (Mie scattering) present in the measurement volume, and on surfaces in proximity to the laser beam. Some filtering of the laser photons may therefore be required. This can be achieved temporally by time-gating or spectrally by suitable filters in front of the detector. In any case care has to be taken to minimize the amount of scattered laser light. Amongst other measures, this can be done by carefully aligning the optics, screening off the laser beam from the detector, matting surfaces and keeping the measurement environment free of dust.

3.1.1 Theory

The fluorescence signal power can be described using the following equation:

$$F = h\nu \frac{\Omega}{4\pi} l A N_1^0 \frac{B_{12}}{B_{12} + B_{21}} \frac{A_{21}}{1 + \frac{I_{sat}^{\nu}}{I_{\nu}}}, \tag{I}$$

where h is Planck's constant; ν, the frequency of the emitted fluorescence; Ω, the collection solid angle; A, the focal area of the laser beam; l, the length of the focal area along the beam; N_1^0, the species population before the laser excitation; B_{12}, B_{21}, A_{21}, the Einstein coefficients for absorption, stimulated emission and spontaneous emission respectively; I_{ν}, the laser spectral irradiance and I_{sat}^{ν}, the saturation spectral irradiance. The saturation spectral irradiance is defined as:

$$I_{sat}^{\nu} \equiv \frac{(A_{21} + Q_{21})c}{B_{12} + B_{21}}, \tag{II}$$

where Q_{21} is the quenching rate constant. Quenching occurs when the excited molecule transfers some or all of its excitation energy to another molecule through collisions. The quenching rate constant is a difficult quantity to evaluate as it is not directly measurable. In most cases the limitations on quantitative measurements are in large parts due to the uncertainties of the quenching rates.

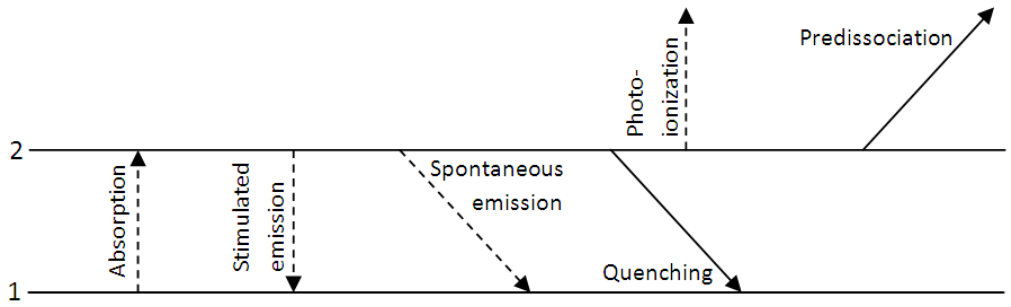

Figure 3-1: A simple two energy level diagram for LIF measurements. The absorption provides a population of molecules excited to the upper energy level and the subsequent spontaneous emission provides the fluorescent signal. All other processes are loss-mechanisms and result in lower fluorescent signal. Figure recreated from reference [10].

In addition to quenching, the fluorescence signal yield is affected by predissociation and photoionization. Though these two last effects are assumed negligible in equation (I), they can be a problem, or even a boon, in certain situations. Where applicable, i.e. where the transition probed is strongly predissociative, one can employ the measurable predissociation rate in order to make the measurements almost independent of the quenching rate. The downside of this is that the signal strength becomes very low due to the signal losses from the predissociation. A similar argument can be made for photoionization. For further details and derivations, the reader is encouraged to consult Eckbreth, chapter 7 [10].

3.1.2 Line-width and broadening effects

The probability for interaction between a photon and a molecule is determined not only by spatial proximity, but also by the spectral overlap of the photon energy and the spectral line-width function of the molecular transition. More precisely the interaction probability is determined by the product of the spectral distribution function of the laser and the spectral line-width function of the molecule, i.e. the overlap of these two distributions. The spectral distribution of the laser is dependent on the type of laser used, and is usually well known prior to any measurement. The spectral line-width function of the molecule is, however, dependent on the conditions within the measurement environment.

3.1.2.1 Natural Line-width

The molecular energy states of the transition probed by the laser comprise a quantum-mechanical system, and thus there is an inherent uncertainty in the energy of these states. This uncertainty is inversely proportional to the lifetime of the energy state [11]. The observable feature from this uncertainty is a statistical distribution of the detectable energy gap of the probed transition, i.e. the peak is broadened according to the lifetime of the energy states involved. The measured peak from an ensemble of probed molecules will have a Lorentzian distribution according to the following equation:

$$f_L(\nu) = \frac{1}{2\pi} \frac{\Gamma}{(\nu - \nu_0)^2 + (\frac{\Gamma}{2})^2}, \tag{III}$$

where f_ν is the line-width function, ν_0 the center frequency of the absorption line, and Γ the inverse of the lifetime of the excited state. This assumes that the lower state is stable, which is most often the case when probing stable, non-radical molecules. The full width at half maximum (FWHM) of the line-width function is Γ. The natural line-width does not depend on ambient conditions.

3.1.2.2 Collisional broadening

Collisions with the emitting molecule will disrupt the emission process and effectively reduce the lifetime of the excited state. This in turn results in a larger uncertainty of the energy of the excited state due to the uncertainty principle. This broadening effect is dependent both on pressure (more colliders) and temperature (faster colliders). The line-width function for collisionally broadened molecules is the same as equation (III), but with a larger Γ due to the further decrease of the excited state lifetime. The broadening effects due to lifetime and collision are called homogeneous broadening as they affect each individual molecule in the same way [12].

3.1.2.3 Doppler broadening

Temperature can be defined as the macroscopic measure of the average kinetic energy of the particles in a volume. Increasing temperature corresponds to an increase in average kinetic energy or speed of the particles. Particles moving towards or away from the light source along the beam path will perceive a Doppler-shift in the photon energy. In an ensemble of molecules this difference in the perceived photon energy for individual molecules manifests itself in a statistical distribution of the absorption energy. This means that the excitation spectrum will get broadened. The emission spectrum will also be broadened because the emitted photons will be Doppler-shifted in a similar manner. Doppler broadening is an inhomogeneous broadening effect as its effect is dependent on the individual molecular kinetic energy [12].

Doppler broadening manifests itself as a Gaussian line shape that can be written with the following equation:

$$f_G(\nu) = \frac{1}{\sqrt{\pi}\Delta\nu_D} e^{-(\frac{\nu-\nu_0}{\Delta\nu_D})^2}$$

The FWHM of a Doppler broadened peak is $\Delta\nu_D$.

3.1.3 Quenching

In LIF measurements the only useful transition the excited molecule can make is a spontaneous emission. No other transition method leads to a signal that can be detected. In quantitative studies it is therefore important to determine the rates of these non-fluorescent transitions. The most difficult rate to determine, and often the most crucial rate, is that of the quenching. Collisional quenching is the non-radiating transfer of energy between colliding molecules. As such, the rates of these transitions are strongly dependent on the pressure, temperature and chemical composition of the ambient gas. In order to determine quantitative LIF measurements one needs to account for the different quenching ratios in regions of the measurement volume where conditions differ. One example of the problems faced in quantitative measurements is that of measurements in a flame. Here it is necessary to account for the temperature gradients and to determine the collision partners in the different regions of the flame. As the combustion process is complex, and there are many intermediate radicals involved, this is not an easy task.

The average quenching rate, Q, can be treated as the sum of the product of the quenching rate coefficients of each molecular species, k_{Qi}, present in the gas and the number density of that species, N_i.

$$Q = \sum_i k_{Qi} N_i$$

The number density is influenced by the pressure, and so the quenching rate is indirectly influenced by pressure as well. Temperature determines the average thermal collision velocity of the colliding species, $\langle v_i \rangle$ according to

$$\langle v_i \rangle = \sqrt{\frac{8kT}{\pi\mu}},$$

where μ is the reduced mass of the colliding species. This in turn influences the species-specific quenching rate coefficient according to:

$$k_{Qi} = \sigma_{Qi} \langle v_i \rangle,$$

where σ_{Qi} is the quenching cross-section.

If the spontaneous emission rate for the probed species is known, it is possible to determine the quenching rate using a short pulsed laser and measure the decay rate of the fluorescence signal [12].

3.2 Detection schemes for ammonia

Only two schemes for the detection of ammonia using LIF that show notable signal strength could be found from the literature. These were LIF using two-photon excitation of the *C'* excited state, and photofragmentation LIF (PFLIF) using single-photon excitation to the *A* excited state and further photofragmentation of the resulting amidogen (NH_2).

3.2.1 Two-photon excitation

In some cases a transition is not achievable using a single-photon excitation scheme. If the transition requires photons of an energy that cannot be achieved, or is difficult to achieve either due to technical or economic considerations, a multi-photon excitation scheme can be used. Most notably this is an issue when the required wavelength goes below ~200nm. In this region only a few laser sources have output of notable strength and the beam will be attenuated by air. Another case where a multi-photon scheme is to be considered is where the transition to be probed is classically forbidden, often due to symmetry rules, e.g. the change in angular momentum is not ±1.

In a two-photon excitation two photons are almost simultaneously absorbed and a transition corresponding to twice the individual photon energy occurs. This process can be viewed as a two-step event. First a photon excites the molecule up to a virtual state. This virtual state has a lifetime given by the Heisenberg uncertainty principle. In a way one can view the photon as being in a superposition of being absorbed by the molecule or not. If a second photon interacts with the molecule within the lifetime of the virtual state, there is a chance that this photon excites the molecule from the virtual state up to a real state. Both photons will in this case be absorbed. If the second photon does not contribute to the excitation, or if a second photon does not interact within the lifetime of the virtual state, both photons will behave as though no interaction occurred at all, i.e. the superposition of the first photon will collapse to not being absorbed by the molecule.

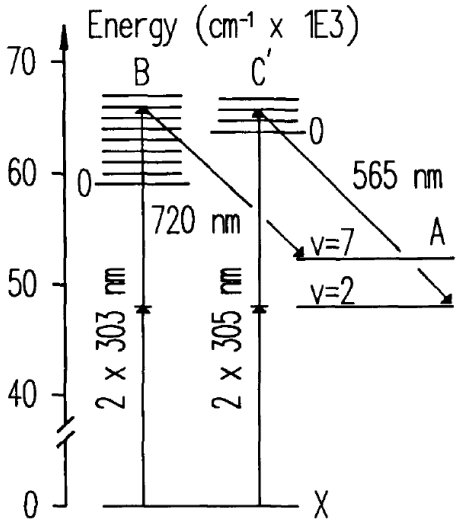

Figure 3-2: Energy level diagram illustrating the two-photon excitation LIF scheme for ammonia. The C'-state shows the strongest signal. Figure from [13].

Although the uncertainty principle indicates that the two photons to be absorbed do not need to interact with the molecule simultaneously, there are limitations to the temporal separation of said photons. In essence this means that in order to increase the chances of a two-photon excitation to happen one need to provide as dense a "cloud" of photons near the molecules as possible. Practically this can be done by focusing the laser beam, i.e. "compressing" the photon cloud perpendicular to the beam; using shorter pulses, i.e. "compressing" the photon cloud parallel to the beam; and increasing the beam power, i.e. providing more photons in total.

The two-photon process has a signal dependence on the laser irradiance of $F \propto I_\nu^2$, as opposed to $F \propto I_\nu$ for the one-photon process [4]. The absorption process happens at much smaller time scales than the duration of the laser pulse. This means that the relevant laser power measure is the mean momentary irradiance and not the time integrated irradiance. In the one-photon process these are the same, but in the two-photon process they are not, i.e. $\langle I_\nu^2 \rangle \neq \langle I_\nu \rangle^2$. This square

dependence on the laser irradiance makes the two-photon process much more sensitive to variations in the beam profile, beam-width variation along the focused area, and laser intensity variations. The modified equation for the two-photon excitation uses the following modified absorption rate constant:

$$W_{12} = \frac{\alpha_{12} I_\nu^2}{h\nu} \tag{IV}$$

When this is inserted into equation (I) the fluorescence signal power can be expressed as:

$$F = h\nu \frac{\Omega}{4\pi} l A N_1^0 \frac{\alpha_{12}}{\alpha_{12} + \alpha_{21}} \frac{A_{21}}{1 + \frac{I_{sat}^\nu}{I_\nu^2}}, \tag{V}$$

where the saturated spectral irradiance now is:

$$I_{sat}^\nu = \frac{(A_{21} + Q_{21}) h\nu}{\alpha_{12} + \alpha_{21}} \tag{VI}$$

For ammonia there are two notable transitions available for LIF detection using two-photon excitation, both originating from the ground state, *X*. One is to the *B* state and the other is to the *C'* state. Both fluoresce through transitions to the *A* state, though to different vibrational levels. The *A* state is strongly predissociative and so the probed molecules is photofragmented in the measurement process [13]. Of the two transitions it has been found that LIF signal from the *X*-*C'* transition is stronger than that from the *X*-*B* transition by two orders of magnitude [13]. The *X*-*C'* was therefore used exclusively during the work for this thesis.

As explained by the Franck-Condon principle [14, 15], transitions between different vibrational states show different cross-sections. The population distribution between different vibrational states in the ground state is dependent on the temperature of the gas and follows the Boltzmann distribution. The experimental data was mostly collected using gas at ambient temperatures, and here the population in the ground state is predominantly in the $X(v_1=0)$ vibrational state. Prior research has found that the strongest transition from the $X(0)$ state to the *C'* state is to the $C(v_2=2)$ vibrational sub-level [13]. Thus the transition subjected to the most scrutiny during the work on this thesis was the $X(0)$-$C'(2)$ transition.

The *C'*-*A* transition shows a strong $\Delta v=0$ rule and the deexcitation transition is thus assumed to be $C'(2)$-$A(2)$. This transition results in a rather broadband fluorescence spectrum due to the short lifetimes of both the involved states and the relatively large amount of rotational sub-levels. The fluorescence signal is centered on 565 nm and extends over 20 nm.

3.2.2 PFLIF

Another viable option for generating fluorescence from ammonia is through photofragmentation. In this scheme the initial molecule is first fragmented through excitation to its predissociative *A* state using an excimer laser at wavelength 193 nm (reaction (a) and (b)). The quantum yield for reaction chain (b) is found to be $\Phi=0.965$ [16]. There are also reports of dissociations to electronically excited amidogen ($NH_2(\tilde{A})$) and to NH [17, 18], though these have yields of 0.024 and ≤ 0.008 respectively. The electronically excited amidogen does, however, not by itself contribute much observable fluorescence in atmospheric conditions due to its relatively long radiative lifetime [19], large quenching rate constant (predominantly electronic quenching) [19] and its broad, almost structureless emission [17].

$$NH_3(\tilde{X},\ v_2'' = 0) + h\nu_{193\,nm} \rightarrow NH_3(\tilde{A},\ v_2' = 6) \quad \text{(a)}$$

$$NH_3(\tilde{A},\ v_2' = 6) \rightarrow NH_2^{\ddagger}(\tilde{X}\,^2\mathrm{B}_1) + H(^2\mathrm{S}) \quad \text{(b)}$$

$$NH_2^{\ddagger}(\tilde{X}\,^2\mathrm{B}_1) + h\nu_{193\,nm} \rightarrow NH_2(2\,^2\mathrm{A}_1) \quad \text{(c)}$$

$$NH_2(2\,^2\mathrm{A}_1) \rightarrow NH(A\,^3\Pi) + H(^2\mathrm{S}) \quad \text{(d)}$$

$$NH(A\,^3\Pi) \rightarrow NH(X\,^3\Sigma^-) + h\nu_{336\,nm} \quad \text{(e)}$$

Following the formation of the internally excited amidogen through reaction (b), a further excitation is induced in reaction (c). Electronically excited NH is then produced through the relatively fast dissociation of the amidogen as shown in reaction (d) [20]. The electronically excited NH fluoresces with the strongest peak centered around 336 nm [17, 20].

The benefit of this scheme when compared to the two-photon excitation scheme is that a much larger cross-section for the generation of LIF is expected. The relatively long-lived intermediate amidogen means that reactions (a) and (c) can be treated as independent on the timescales of a laser pulse. It has been indicated that the strength of the LIF signal from NH show a quadratic dependence on the laser fluence, but that each of the transitions involved ((a) and (c)) have a linear dependence on the laser fluence separately [20]. As opposed to the two-photon excitation, which shows a dependence on the mean momentary irradiance ($\langle I_\nu^2 \rangle$), the PFLIF should show a dependence on the time integrated irradiance ($\langle I_\nu \rangle^2$). This is due to the allowable time-separation between the two transitions involved being greater than the duration of the laser pulse.

Another benefit to the PFLIF scheme is that the excimer lasers used can reach very high output power when compared to frequency doubled dye-lasers. Excimer laser are also more stable and robust, and even though their beam-profile is not on par with a properly aligned pumped dye-laser, the increase in beam power more than makes up for it. The increased power coupled with the signals quadratic dependence on laser fluence further elevates the benefits of using an excimer laser.

A downside to this method of generating fluorescence signals is that it requires the input of laser light below 200 nm. In this region attenuation of the beam both by air and combustion species is a noted problem [21]. The increased potential for photoionization and photolysis of other species than ammonia is also present. This may in some cases influence the measured system or environment to such a degree that the technique cannot be regarded as non-intrusive.

3.3 Concentration measurements

The measured signal intensity in LIF measurements is dependent on the amount of molecules within the irradiated volume. The measurements thus show the *density* of molecules belonging to the probed species and not the *concentration* of the species. In an ideal case with no temperature and pressure variations in the measurement volume, the LIF measurements give qualitative data that corresponds to the concentration of the species. In most cases, where there are temperature and pressure variations, variations in the density of the gas and the quenching rates influence the measurements. Providing quantitative concentration measurements in environments with large pressure and/or temperature gradients is therefore difficult.

3.3.1 Parameters for concentration measurements

In order to accurately determine concentrations when using LIF measurements, it is necessary to determine several factors.

- Temperature: The temperature dependence of the LIF signal needs to be known if the measurement environment has temperature gradients. It is sometimes possible to identify an absorption line that is relatively stable with temperature changes thus minimizing the problem of unknown temperature variations. It is in any case necessary to determine the temperature distribution in the measurement environment in order to account for the density variations these entail.
- Pressure: The pressure of the measurement environment influences the quenching rates, pressure broadening and number density, which in turn influence the LIF signal. It is therefore necessary to determine the pressure, and pressure gradients if present.
- Gas composition: The quenching rate and pressure broadening are both dependent on the collision partners present in the probed gas volume. In order to account for these effects it is necessary to determine the molecular composition of the gas in the measurement environment. In flame measurements this adds additional problems as the gas composition changes across the flame front.
- Beam attenuation: As the laser beam passes through a gas, it gets attenuated. This influences the measurement as molecules further downstream the beam see a lower irradiance than molecules upstream. The result is a slight signal strength gradient running parallel to the beam when measured in a homogeneous gas mixture. This effect can be accounted for either by calculation of the attenuation, or by calibration using direct measurements in a homogeneous gas.

In cases where the measurement environment is enclosed, it is often possible to calibrate the concentration measurements by filling the volume with a known gas composition, and measure the LIF signal from this.

3.4 Setup

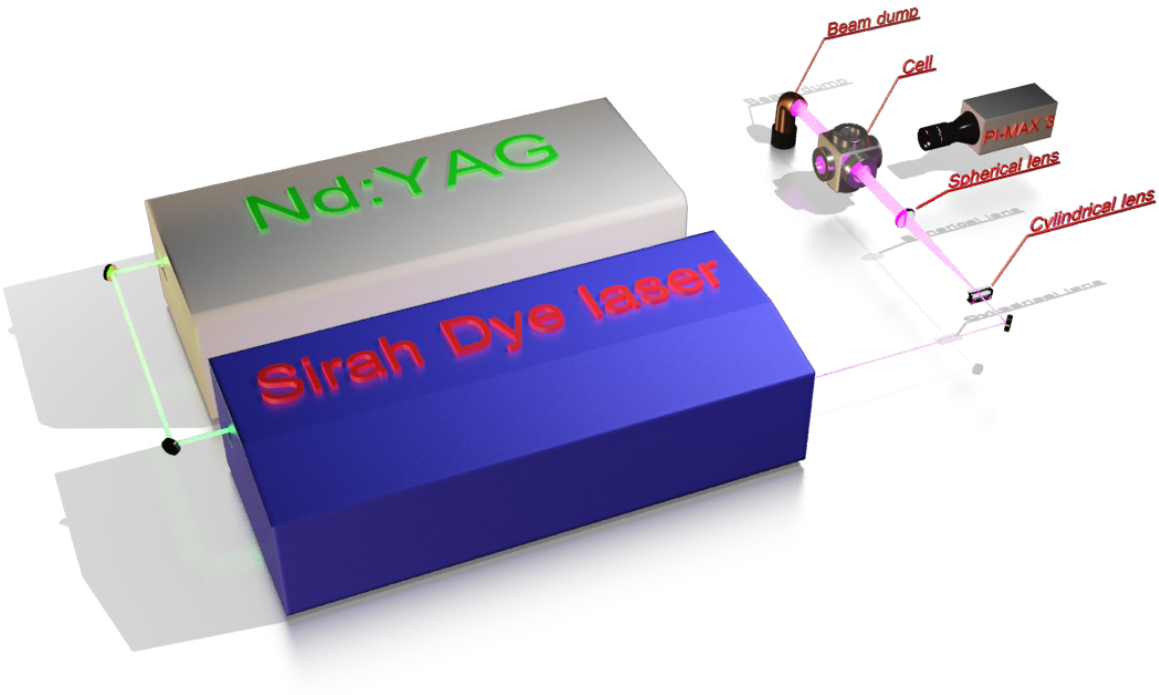

Figure 3-3: Basic setup for LIF measurements

The basic setup for LIF measurements consists of a (pulsed) laser, focusing optics, beam dump and a detector. For 2-d imaging measurements (PLIF) the detector is a camera, usually an intensified CCD-camera, and the focusing optics for a laser-sheet by combining cylindrical and spherical lenses. Detector and laser are linked, either directly or through a control unit, to ensure that the detector measures during a short interval only when the laser pulse is fired. The time gate can be adjusted to minimize scattered laser light by setting its starting point to just after the laser pulse has passed through the measurements volume. The time gate should be as short as possible to remove background light, but it should still be long enough to capture most of the LIF signal.

In non-resonant LIF, where the laser wavelength is notably different from the fluorescence wavelength, filters are often used to remove scattered laser light. The benefit of this is that more of the LIF signal can be collected as the time gate can overlap with the laser pulse. In point-wise measurements the detector is often a PM-tube (Photo Multiplication-tube), and the LIF signal is collected using a large spherical lens between the measurement volume and the PM-tube.

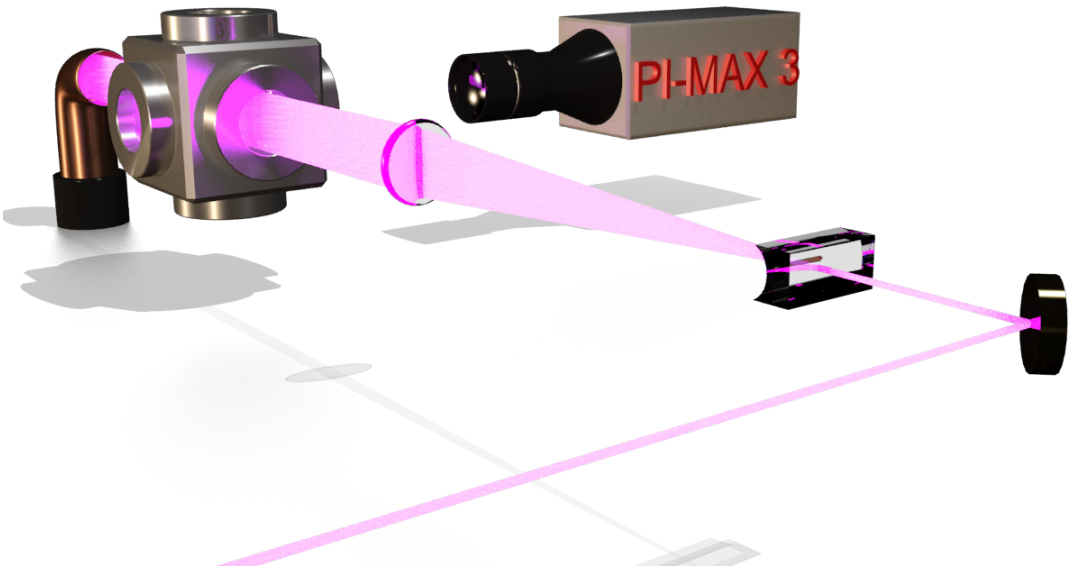

Figure 3-4: Constructing a laser sheet using a concave cylindrical lens and a convex spherical lens

A laser-sheet can be constructed in several ways, though the easiest method, requiring the fewest lenses, consist of one cylindrical lens expanding the beam in one plane and a spherical lens to collimate the beam in the same plane and focus it in the other. The height of the sheet made in such a way is determined by the focal lengths of the lenses used. If the beam diameter is D, the cylindrical lens has a focal length of f_1 and the spherical lens has focal length f_2, the laser sheet height, H_{ls}, is given by:

$$H_{ls} = D\left|\frac{f_2}{f_1}\right|$$

4 Absorption spectroscopy

Absorption measurements are viable for determining the concentrations of ammonia in a gas-mixture. These measurements are much more sensitive than LIF measurements, but do not provide possibility for imaging. The basic procedure of these techniques consists of measuring the attenuation (decrease) of light as it passes through a gas volume. By using a light source that emits photons of a specific wavelength, the technique can be species specific as the wavelengths absorbed by molecules are discrete. Care must be taken when choosing the wavelength, however, so that only the species of interest absorb the photons. Another important consideration is the strengths of the transitions. In the end a compromise often needs to be made between transition strength and absorption overlap from other species [22]

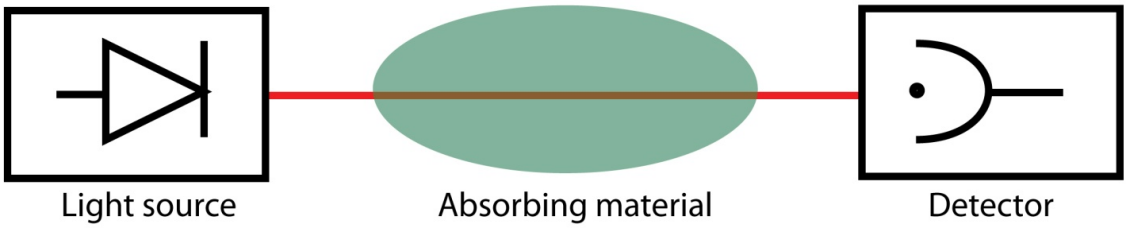

Figure 4-1: A simple model of absorption measurements. Using a laser light source enables the measurements to have some spatial information. The laser beam could for example pass through a flame at a certain height above the burner and so give information on the absorbance of the gas within the flame at that height. Note that the measurements in the case of absorption are always integrated along the total beam path. Figure from ref [22].

In the case of ammonia there is very strong absorption in the UV-region from 213 nm and below. These wavelengths are impractical to use however, as they require expensive and large laser systems. Diode-lasers are the more practical and cheap alternative, but these are not yet commercially available at these wavelengths [23]. The alternative then is to use the absorption features found in the IR-region above 1800 nm. The largest absorption cross-sections by ammonia in the IR-region can be found between 1900 nm and 2050 nm, but this region also shows absorption by water and CO_2 (see Figure 4-2).

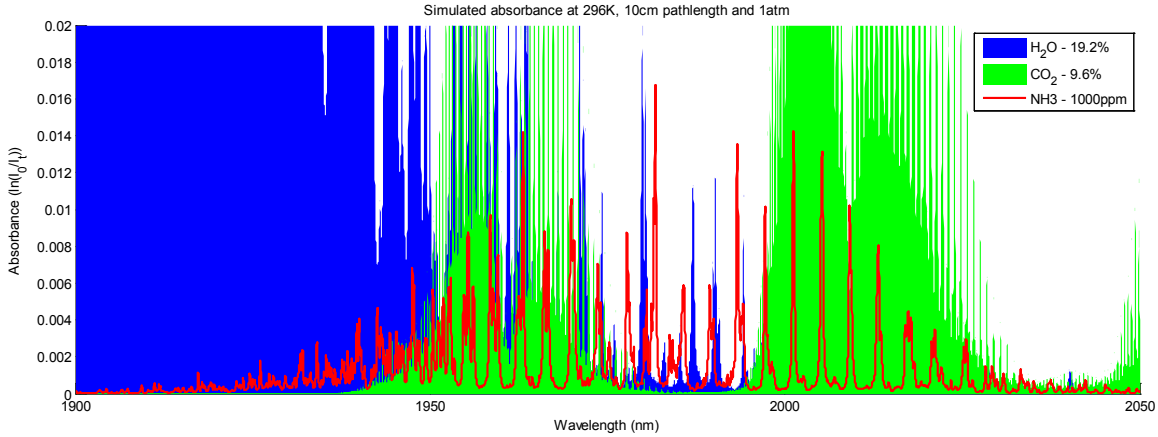

Figure 4-2: This spectrum shows a comparison between the absorption from water, CO_2 and ammonia. The data used is from the HITRAN database. The ammonia absorption lines overlap with water and/or CO_2-lines throughout the region. There is a small region around 1990 nm where the overlapping lines are weak compared to the ammonia lines. Some of these ammonia lines could thus be candidates for probing.

Other absorption features by ammonia can be found between 2200 nm and 2300 nm and this region shows no significant absorption by other species. Diode-lasers in the IR-region are commercially available.

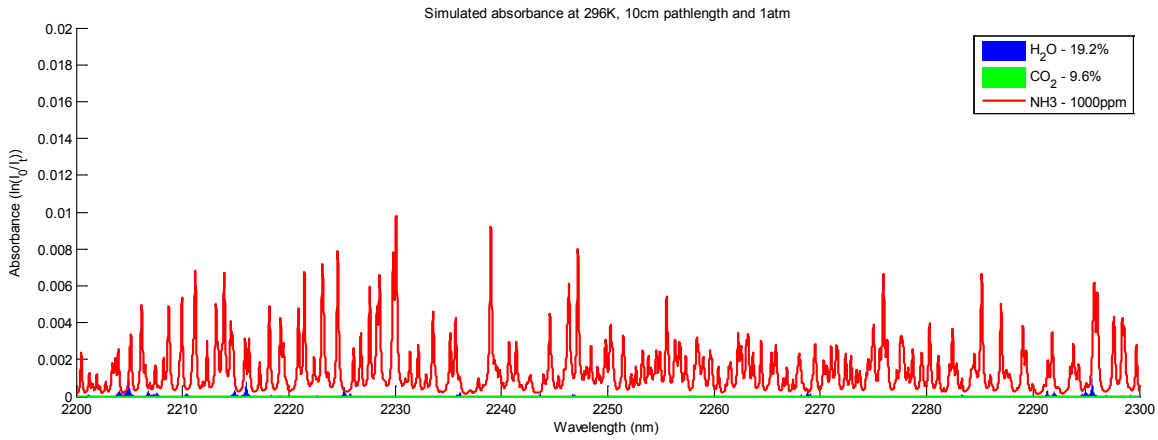

Figure 4-3: This spectrum shows a comparison between the absorption from water, CO_2 and ammonia. The data used is from the HITRAN database. This region shows almost no water and CO_2-lines and the few lines that are there are very weak. Several ammonia absorption lines have been identified in this region as suitable for probing. Observe that the absorbance in this region is generally lower than in the region plotted in Figure 4-2.

Suitable absorption lines in the above regions have been identified and their temperature dependence, transition intensities and proximity to absorption lines from other species have been evaluated. For further details on absorption based detection techniques see [22].

4.1 Suitable spectral lines for probing

Absorption lines that could be used for concentration measurements need to be discernible from absorption features of other species, in combustion applications the most notable other species are water and CO_2. The probed line should also be relatively stable with temperature within the expected temperature range of the measurements. Finally the absorption line used should have a high absorption cross-section so that the signal, and thus the lower detection limit, is as good as possible.

It has been reported that sub-ppm concentration measurements of ammonia are achievable using absorption lines of comparable transition strengths to those presented in Table 4-1 [24, 25].

Table 4-1: Red marked lines have a good balance between line intensity and stability. Green marked lines have very low overlap with other lines.

Temperature stability (rank)	*Wavelength [nm]*
1	2307.73
2	2206.14
3	2208.66
4	2213.93
5	2223.16
6	2305.52
7	2230.10
8	2239.00
9	1993.23

A plot showing the temperature stability of the above lines can be found in Appendix A together with simulated spectra centered on each individual line.

5 Results and analysis

The main part of the experimental work consisted of determining the relevant parameters influencing the generation of LIF using the two-photon excitation scheme outlined in section 3.2.1. This scheme had already been used to measure two-dimensional images of ammonia by Georgiev and Aldén [4], though at much higher concentrations than presented in this work. The lower detection limits when imaging ammonia in non-flame and flame environments was investigated, and the technique was applied to measure the dynamics of ammonia seeded in a flame as well as above an ammonia-oxidizing catalyst sample.

5.1 Laser

The laser used in the measurements consisted of a dye laser (Cobra Stretch-G-2400, Sirah) pumped by an Nd:YAG (Quanta-Ray PRO 250-10, Spectra Physics) laser at 532 nm operating at 10 Hz repetition rate and with 8 ns pulse duration. The dye used was a mixture of Rhodamine 610 and Rhodamine 640 optimized for output at 609 nm. The output beam was then frequency doubled using a BBO crystal resulting in a beam in the UV region at approximately 304.5 nm. The beam profile was measured in order to accurately determine the size of the focal region used during measurements. The results of this measurement are given in Figure 5-1.

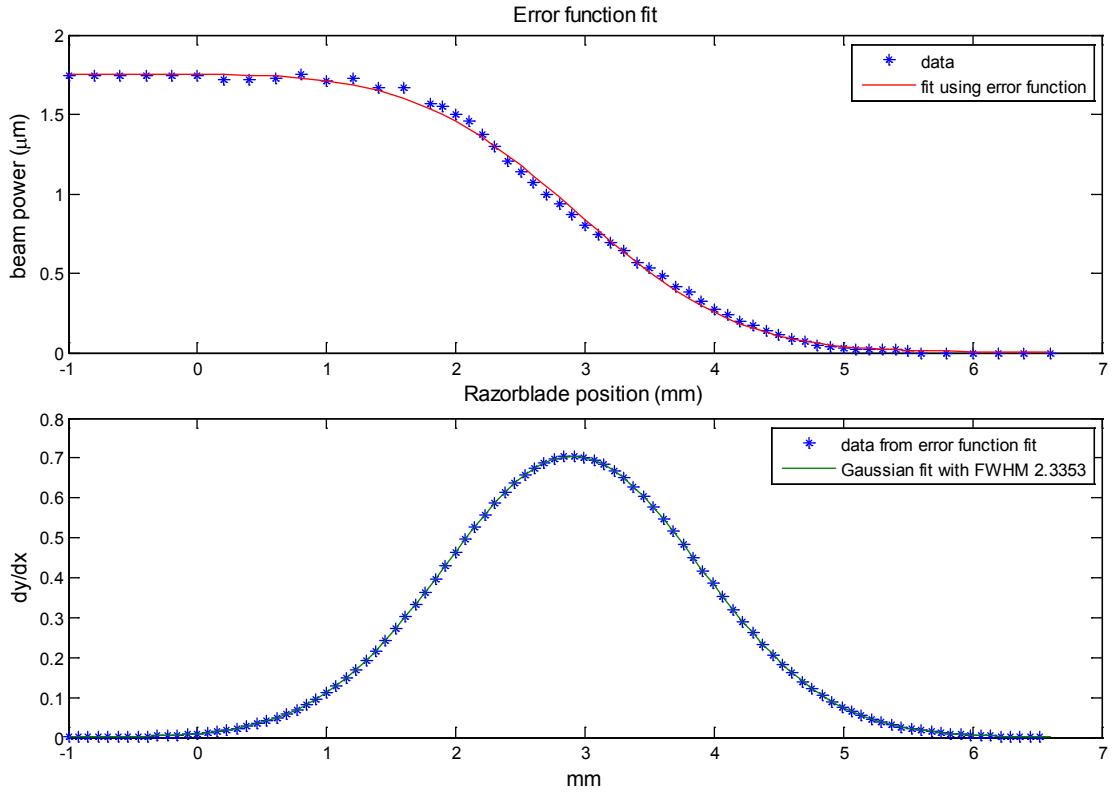

Figure 5-1: Analysis of beam profile of the frequency doubled laser beam emitted from the Sirah dye-laser system. The initial data points (blue asterix top graph) were measured by incrementally covering the unfocused laser beam with a vertical razor blade and measuring the beam power. The unfocused beam was used because the focused beam perforated the razor blade. The beam power is in µJ, the relatively low power was used to minimize damage to the detector and the razor blade. Assuming a Gaussian shape for the beam profile, the top plot should follow a curve described by the integral of a Gaussian curve, i.e. by the error function ("erf" in Matlab). A 4-parameter fitting algorithm was used to fit the error function to the data. The data in the lower plot is the (numerical) derivative of the fitted error function. These data points were then fitted to a Gaussian curve and the FWHM is extracted directly from the resulting parameters describing the curve.

As can be seen from Figure 5-1 the beam shows a good fit with a Gaussian profile and has a FWHM (Full Width at Half Maximum) of approximately 2.3 mm. This figure was used to estimate the widths of the laser-sheets mentioned throughout this chapter.

Due to quadratic dependence on the irradiance for LIF signals, the central parts of the laser-sheets showed much larger signal than the wings. The wings were therefore cropped using an aperture and, where possible, the signal variations due to the beam profile was removed through normalization.

5.2 Power dependence

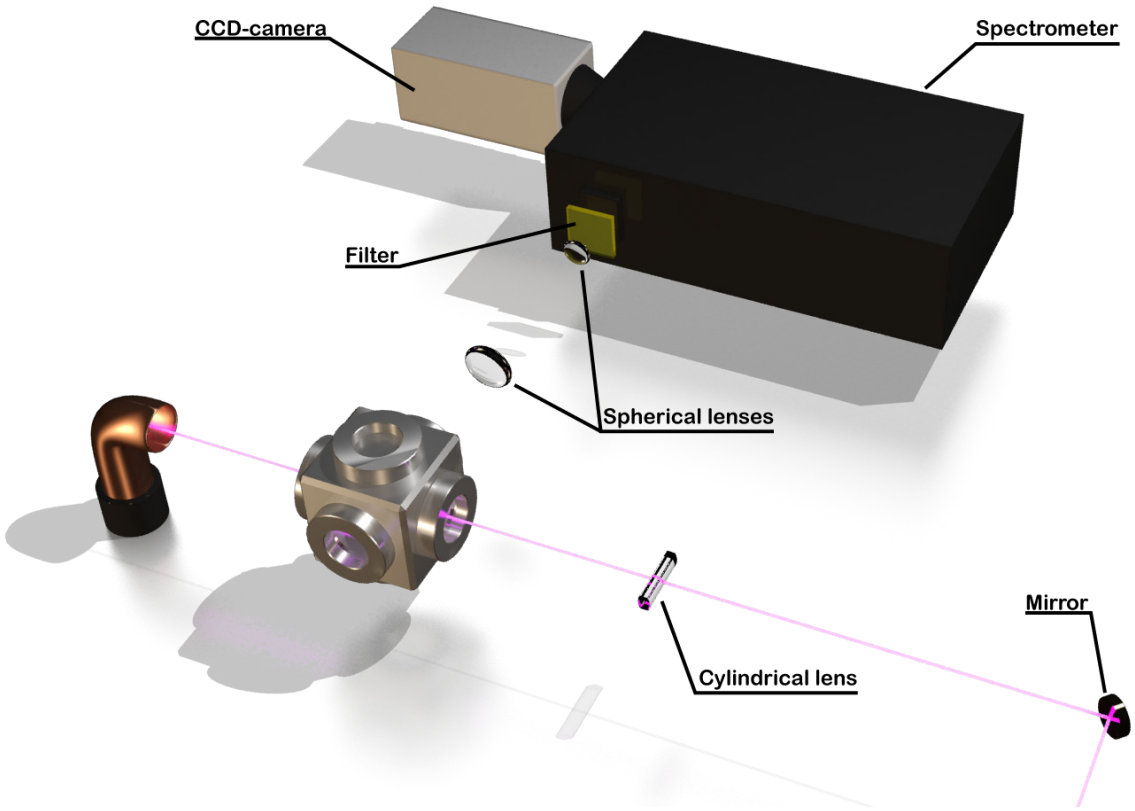

Figure 5-2: Setup used for evaluating the power dependence of the LIF signal.

The measurements were carried out by passing the laser beam through a stainless steel pressure cell with fused silica windows filled with pure ammonia gas at room temperature and ambient pressure. The beam was focused using a cylindrical lens with focal length f=300 mm (measured focal length was 280 mm due to chromatic aberration). The focal point of the beam was in the center of the pressure cell cavity. The fluorescence was collected on the entrance slit of a spectrometer (Acton SpectraPro 2500, grating 1200 grooves/mm, blaze 300 nm) using two spherical lenses (f=152 mm and f=37 mm). A high-pass filter of type Schott GG400 was placed in front of the slit to suppress scattered laser light. The spectrometer was in conjunction with a Princeton Instruments PI-MAX III CCD camera. The output laser energy was measured at 22 mJ and this was adjusted by passing the beam through a Newport beam attenuator prior to the focusing cylindrical lens. The laser was set at 609.58 nm as this was measured to give the strongest LIF signal.

As mentioned in section 3.2.1, the two-photon excitation scheme means that the fluorescence signal scales with the square of the laser irradiance. This is, however, only true at low levels of laser irradiance where $I_\nu^2 \ll I_{sat}$ as this makes it valid to approximate equation (V) to ("quadratic regime"):

$$F = h\nu \frac{\Omega}{4\pi} l A N_1^0 \alpha_{12} I_\nu^2 \frac{A_{21}}{(A_{21} + Q_{21})\hbar\omega} \qquad \text{(VII)}$$

At higher laser irradiance the complete equation (V) needs to be used. At very high irradiances where $I_\nu^2 \gg I_{sat}$ equation (V) can be approximated to ("saturated regime"):

$$F = h\nu \frac{\Omega}{4\pi} l A N_1^0 A_{12} \frac{\alpha_{12}}{\alpha_{12} + \alpha_{21}}, \qquad \text{(VIII)}$$

i.e. the fluorescence signal is independent of both irradiance and quenching. These levels of irradiance are impractical to reach in two-photon excitation schemes and equation (VIII) is only mentioned as an extreme case useful for explaining the results.

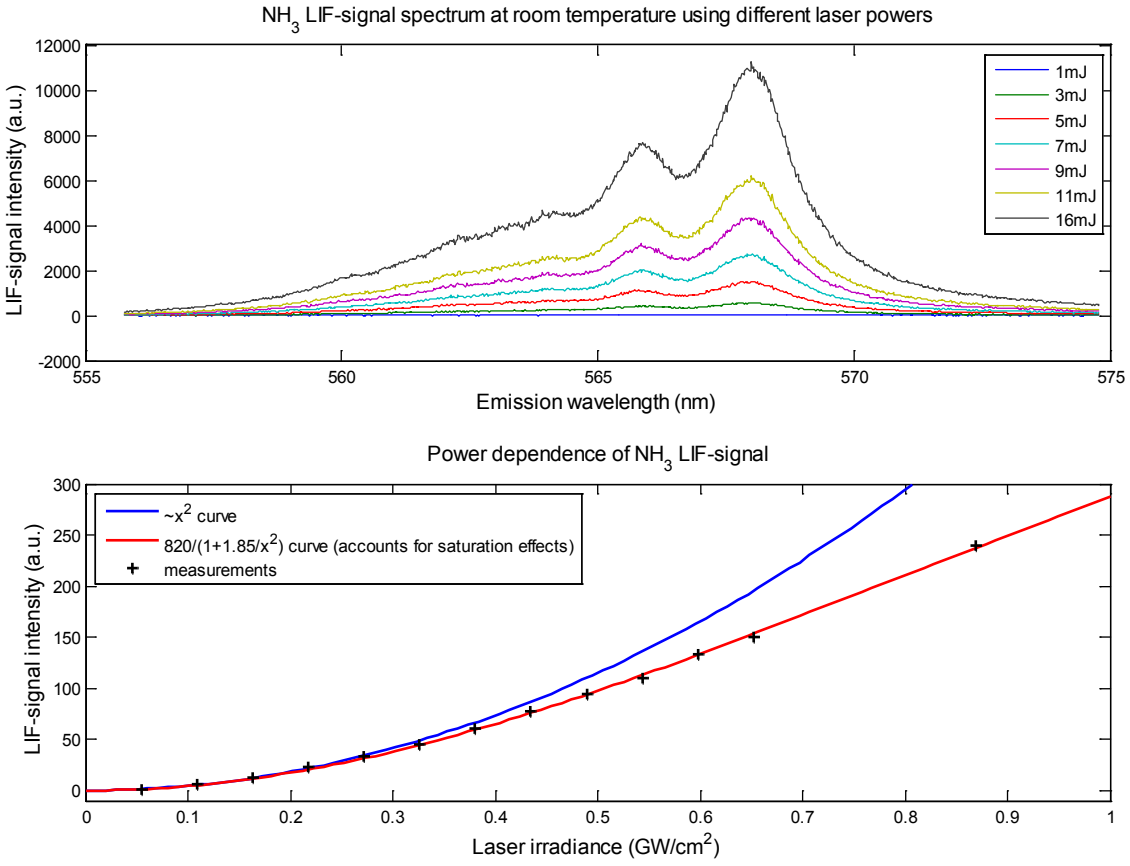

Figure 5-3: Analysis of the power dependence of the fluorescence signal on the incident laser energy. The top part of the figure shows the emission spectrum observed using a laser output wavelength of 304.79 nm (strongest observed signal). The emission spectrum is quite broad and smooth which is due to the short lifetimes of the excited *C'*-state and the predissociative *A*-state. The lower part of the figure shows the power dependence of the LIF signal. The blue curve shows a quadratic function fitted to the first 5 measurement points. The red curve shows a fitted curve using equation (V) with two fitting parameters. For calculations of irradiance, the focused area was determined to be approximately 0.1×2.3 mm.

The energy was measured using a laser power meter measuring the power in Watts. As the laser is running at 10Hz, it is simply a matter of dividing the power with the frequency to find the energy of each laser pulse in Joule. From section 5.1 the laser beam width is known and the size of the focus can be calculated. With knowledge of the average duration of each pulse and the area illuminated (the focus) one can estimate the laser irradiance. Using the unit irradiance makes it possible to compare the above figure with that of the power dependence of the stimulated emission (section 5.6).

As expected for low energies, the signal intensity has a quadratic dependence in the laser power. As the energy increases the quadratic curve (blue) starts to deviate from the measurements. This is mainly due to three effects:

1. Saturation: Saturation happens when the rates of absorption and stimulated emission become so large that they completely dominate the energy transfer into and out of the upper state [10].
2. Amplified Spontaneous Emission: This effect will be further discussed in section 5.6. This effect is a cascade of stimulated transitions that are caused by spontaneous emissions from the excited molecules. This cascade is directed mostly along the laser path and does not reach the detector.
3. Dissociation: The excited molecule can dissociate, i.e. break apart, instead of radiating the excess energy by transitioning to a lower state. This process cannot be detected in the setup used for LIF as no photon is released. The dissociation is probably a small effect as is requires further excitations of the already excited molecules. These further excitations may also ionize the molecule through photoionization. The spontaneous dissociation rate of the upper state of ammonia is an inherent property of the molecule and does not depend on the laser irradiance.

These effects all compete with spontaneous emission to remove the population of excited molecules. Since we only detect the spontaneously emitted photons, the other effects "steal" from the signal. At some point, equilibrium between losses and gains with increasing irradiance will be achieved. At this point further increase of the laser irradiance will not increase the signal, and in some cases even lower it.

In the energy region accessible during the measurements this equilibrium cannot be seen, but the red curve is slowly transitioning to it. Thus, the blue curve corresponds to the low energy approximation given in equation (VII), while the red curve corresponds to the more complete description as given in equation (V). For sufficiently high laser power it is expected that the power dependence reaches the saturated regime as described by equation (VIII), but at these levels of laser irradiance other effects such as optical breakdown (ionization of the gas within the focal area) and amplified spontaneous emission (see section 5.6) needs to be considered as well.

5.3 Concentration dependence

Concentration dependence was determined by flame measurements using a conical water-cooled stainless-steel Bunsen-type burner. Ammonia was seeded into the fuel so that the fuel/ammonia ratio could be adjusted between measurement points. The laser power was measured to 10 mJ with a Gentec power meter fitted with a diffuser with a measured attenuation factor of 3.75. The output power from the laser was thus 38 mJ. The laser beam was shaped to a sheet, with the focal point in the centre of the flame cone, using a cylindrical lens (f=-100 mm) and a spherical lens (f=300 mm) giving a sheet width around 20 mm. The LIF signal was collected with a Princeton

Instruments PI-MAX III intensified CCD camera, fitted with a B Halle (*f*=150 mm, *f*/2.5) objective and a Schott GG495 filter, mounted perpendicularly to the laser beam.

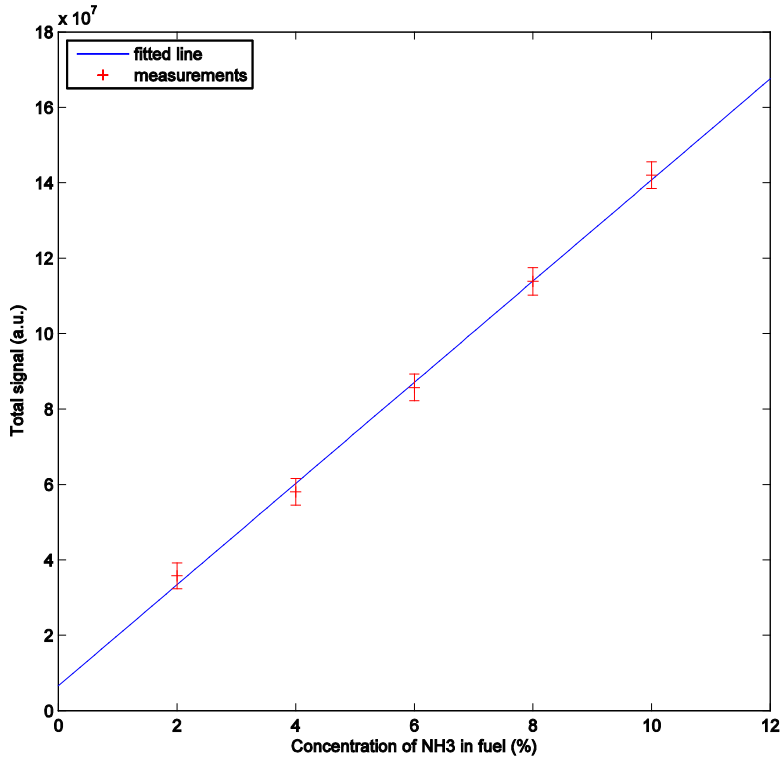

Figure 5-4: LIF signal vs. concentration of ammonia in fuel. A premixed flame with approximate stoichiometry of Φ=1.2 was used due to stability issues with lower Φ at the higher ammonia concentrations. Three Bronkhorst flow controllers were used to set the ratios of air, ammonia and methane to the ratios given in Table 5-1. The error bars are predominantly due to the accuracy of the flow controllers. A clear linear relationship is observed

Table 5-1: Flow rates of ammonia, methane and air in premixed flame. The Φ values are calculated using a stoichiometric ratio based on the fuel used in each measurement. This stoichiometric ratio differs from a pure methane/air flame and is slightly different for each of the fuel mixing ratios given.

NH_3 (% of fuel)	NH_3 (l/min)	CH_4 (l/min)	Air (l/min)	Φ
10	0.069	0.63	5.3	1.17
8	0.055	0.64	5.3	1.19
6	0.041	0.66	5.3	1.21
4	0.027	0.67	5.3	1.22
2	0.013	0.68	5.3	1.24

In LIF measurements the relevant gas-measure is not really concentration, but number density, i.e. how many absorbing molecules there are for a given volume. If the temperature increases in a homogenous gas mixture, the number density decreases and if pressure increases, the number density increase. By necessity then, the measurement environment needs to be relatively homogenous in temperature and pressure in order to do quantitative concentration measurements. Under the same pressure and temperature conditions, however, the number density is proportional to the concentration.

5.4 Pressure dependence

The pressure dependence measurements used the same setup as the power dependence measurements except that the beam attenuator was removed. The pressure was manually adjusted and measured by a digital pressure meter with 0.01 bar precision.

As mentioned in section 5.3 pressure will influence the signal by influencing the volume number density. There are, however, other effects of pressure that also influence the fluorescent signal. These mostly decrease the signal with increasing pressure and so oppose the general signal increase attributed to the increase in volume number density. One such effect is pressure broadening. The broadening effects result in a smaller spectral overlap between the laser spectral distribution and the absorption feature. This means that fewer molecules are available to absorb the laser photons and thus fewer molecules yield fluorescent emission resulting in a lower signal.

Another process affected by pressure is stimulated emission. This process is further described in section 5.6. This effect also results in an overall loss of signal as the stimulated emission competes with the spontaneous emission process.

Increasing the pressure will also increase the quenching rate. Quenching is non-radiative transfer of energy between molecules in the measurement volume. As the lifetime of the excited state of ammonia is short, quenching is considered to contribute a relatively small signal loss at atmospheric pressures, but the results indicate that quenching gives significant signal losses at higher pressures.

In the case of ammonia the combined effects of broadening and quenching result in a decrease of the signal with pressure.

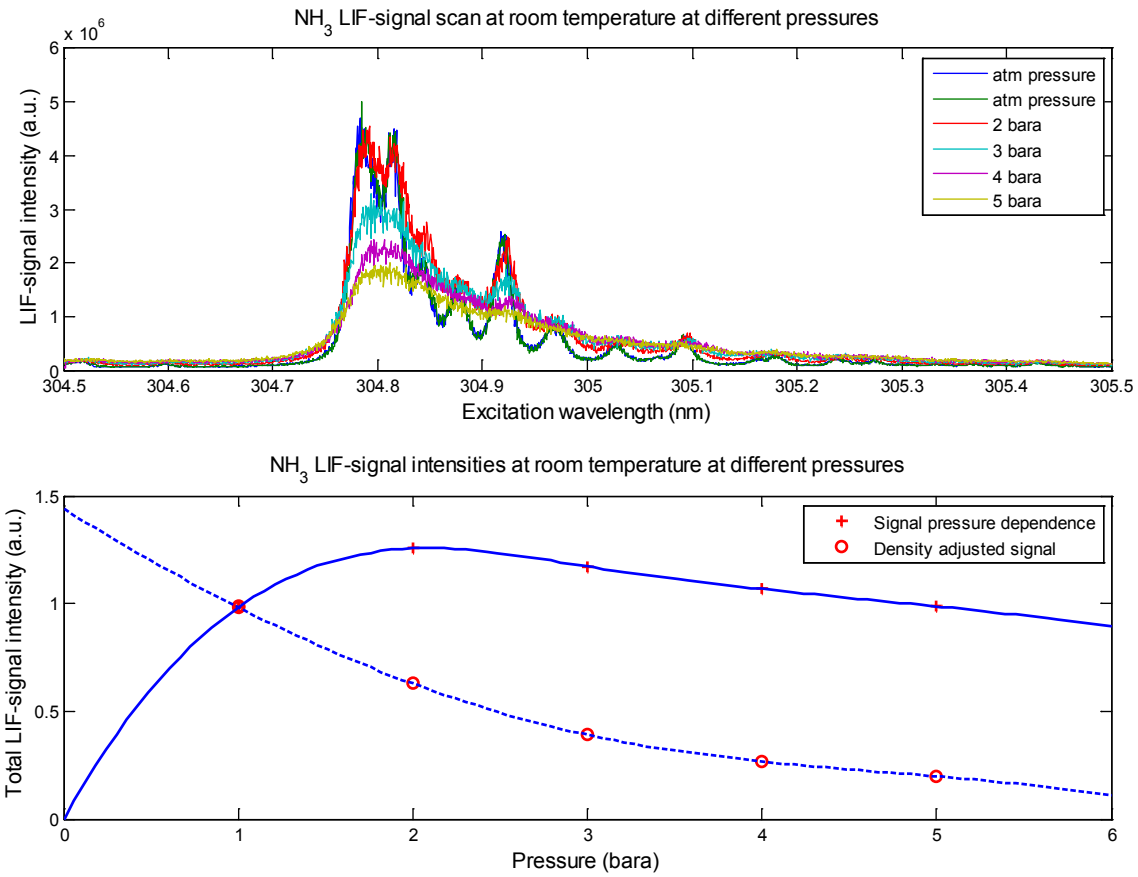

Figure 5-5: The pressure dependence of the signal strength. The top half shows excitation scans at different pressures. As can be seen there is significant broadening of the peaks as pressure increases. This broadening is due to pressure broadening. A very slight line shift can also be observed, most notable on the peak just above 304.9 nm. The overall decrease in signal intensity is likely mostly due to quenching. The pressure increase corresponds linearly to an increase in the number density of ammonia. This in turn gives an increase in the emitted fluorescent signal that is due to the increase in number density and not the pressure itself. The circles in the lower plot in the figure have been normalized to show the expected intensity variation with pressure independent of the number density variations. The blue lines in the lower plot are just to guide the eyes.

5.5 Temperature dependence

The temperature measurements used a similar setup to the power dependence measurements. The cell was replaced with a smaller one that had heating ribbons on the outside and a thermocouple type K mounted inside. The laser beam was focused using a cylindrical lens (f=100 mm). The cell was filled with pure ammonia gas, heated and the pressure equalized to ambient pressure at each measurement point by quickly opening and then closing the outlet valve. The laser output energy was measured to 23 mJ, but dropped to 20 mJ during the latter stages of the measurements. The filter in front of the spectrometer slit was replaced with a Schott GG495 filter to further suppress scattered laser light. At each measurement point the dye laser was scanned from 304.5-305.5 nm at 0.005 nm/min. An accumulated measurement using the resonant wavelength at 304.79 nm was also carried out for each measurement point.

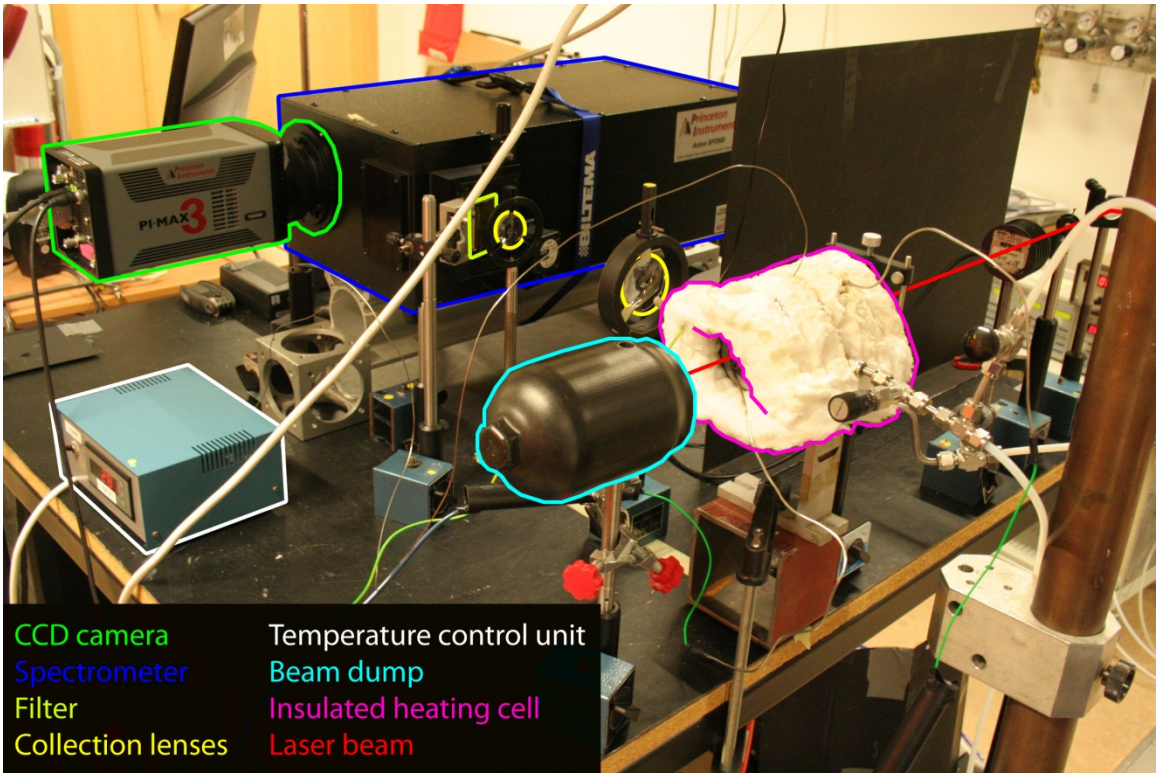

Figure 5-6: Image showing parts of the setup used for determining the temperature dependence of the LIF signal.

The LIF signal can have a complex dependence on temperature. On the one hand the local temperature and pressure determines the number density and thus the signal strength in a direct way. Increasing temperature corresponds to an expansion of the gas and thus a lower number density. On the other hand temperature influences the signal strength in several other ways:

1. Doppler broadening. Doppler-broadening results in a decrease in signal strength if the spectral width of the laser is shorter than the spectral width of the broadening.
2. Collision broadening. As mentioned in section 3.1.2.2 collisional broadening is influenced by temperature as the average speed of the particles will influence the collision rate.

3. Population distribution. Temperature will influence the distribution of the states within the system. In short the translational kinetic energy is distributed among all degrees of freedom inherent in the particles through interactions. For molecules with more than one atom these degrees of freedom include rotational and vibrational motions. These rotation and vibration modes are discrete and correspond to rotational and vibrational states. Increasing temperature will shift the distribution of these states to populate higher energy states. This will influence the transition strengths as the lower level population will change. Some transitions will get stronger and others will get weaker with temperature.

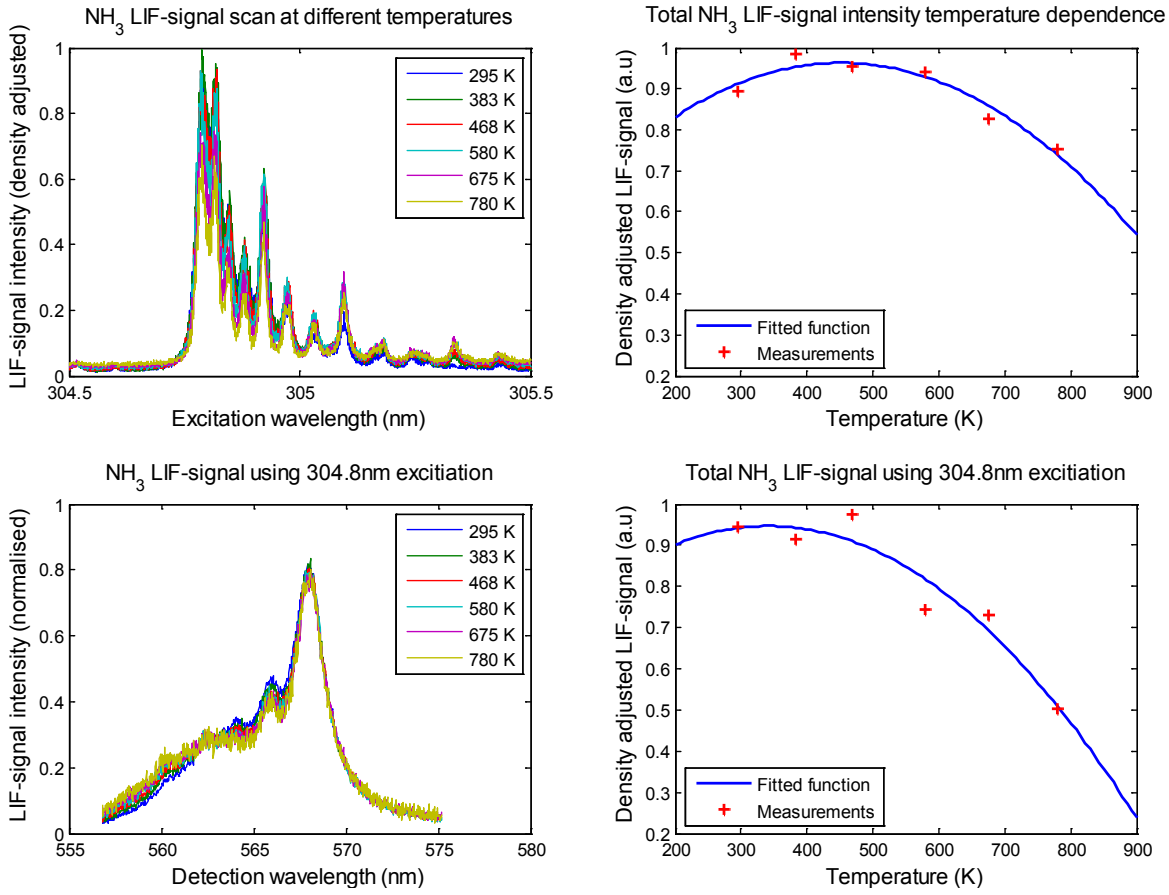

Figure 5-7: Figure showing the temperature dependence of the C'-X transition in ammonia. Top left: excitation scans at different temperatures. The signal strengths have been adjusted to account for number density variations with temperature. Observe that there is no noticeable broadening of the spectrum, indicating that collisional and Doppler-broadening effects are not resolvable due to the laser spectral width and the complex rotational structure of the transition. The transition strength also shifts towards higher wavelengths with temperature. Top right: integral of the excitation scans in top left. The total signal decrease at higher temperatures. Bottom left: emission spectra at different temperatures. The spectra are normalized with their integral. Bottom right: integral of the emission spectra in bottom left. The total signal decreases rapidly at higher temperatures.

From Figure 5-5 it is clear that the signal strength decreases at higher temperatures. In environments with sharp and turbulent temperature gradients this will result in uncertainties in the measurements. In environments with stable flow conditions the effects of temperature gradients can to a large part be accounted for by calibration measurements.

5.5.1 PGopher simulation

Using the data from the temperature excitation scans a contour fit was made for each spectrum. This was done using the program PGopher [26]. The starting point was using constants for the transition $X(0)$-$C'(0)$ available from the PGopher support page. In this simulation the point group is assigned as D_{3h} due to the hydrogen atoms in the ammonia molecule being able to tunnel through the plane of inversion. This inversion results in a splitting of the (redundant) vibrational levels into v^+ and v^-. Due to the planar nature of the excited states these also belong to the D_{3h} point group. This means that both states involved in the transition have the additional symmetry of reflection in the plane. The v^+ and v^- levels in the ground state will then influence the transition energy depending on whether the final state is inverted from the initial or not [27].

Using prior determinations of the molecular constants of the $C'(0)$ and $C'(1)$ states [7, 27], an initial estimation of the constants for the $C'(2)$ state was made. After refinement of this initial estimation using the temperature excitation scans as overlays, successive fitting to the contour of the scans was carried out. After several iterations of fitting, each iteration adding more parameters, a relatively good fit for the experimental data was obtained. This fit has a good agreement with the measured data across all the temperature and can be used to estimate the behavior of the transition for any temperature. The final parameters obtained through this work are presented in Table 5-2.

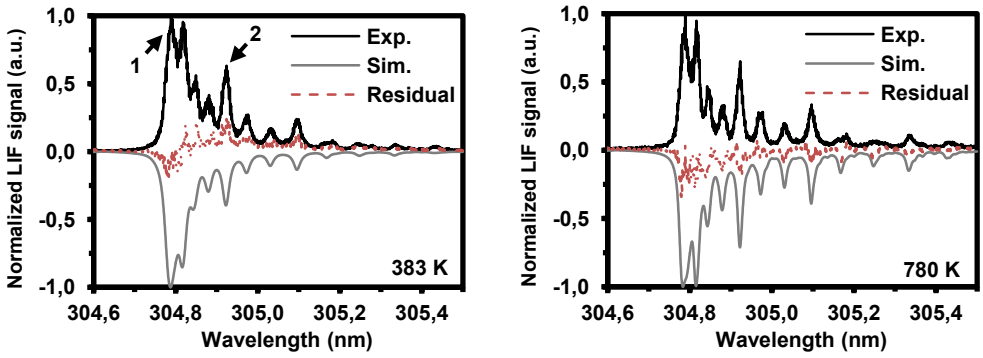

Figure 5-8: Graphs showing the experimental and simulated excitation spectra for two temperatures. In the left graph two peaks are indicated. Peak 1 is the peak used for most of the work in this thesis as this has the highest signal. Peak 2 was identified as having a lower dependence on temperature over the interval 400-600 K. In situations where temperature stability is of importance, peak 2 might be a better choice for LIF measurements. It can be shown by extrapolating the simulation to higher temperatures that the signal continues to decrease and that peak 1 and 2 approach each other in intensity.

Table 5-2: Spectroscopic parameters of the *C'*(v'=2) state in cm^{-1} obtained through contour fitting of the spectra. For comparison the literature values for the v'=0 and v'=1 vibrational levels are also shown. *: Data from ref [27]. **: Data from ref [7]

Constant	***v'=2***	***v'=1***	***v'=0***
Band origin	65598.16	64710.41 (0.05)* 64709.49**	63866.397 (0.028)* 63865.62**
B	10.041	10.332 (0.001)* 10.323**	10.770 (0.001)* 10.778**
C	5.40	5.281 (0.001)* 5.322**	5.229 (0.0009)* 5.264**
10^6D_J	1636	-287 (8)* 416**	242 (8)* 1091**
10^6D_{JK}	-2462	744 (9)* -541**	-588 (12)* -2043**
10^6D_K	867	607 (11)* 36**	211 (15)* 910**

5.6 Stimulated emission and Amplified spontaneous emission

Stimulated emission occurs when an incoming photon induces a transition in an excited molecule. The emitted photon will have the same phase and energy as the incoming photon due to the bosonic nature of photons. In the case of a one-photon excitation scheme the stimulated emission is dominated by emissions induced by the incoming laser photons themselves. As the rates for absorption and stimulated emission are the same, this result in an upper boundary to the population of the upper state (saturation). In the case of multi-photon excitation schemes the original transition is forbidden by single-photon emission. The excited state will instead transit to another state, not the ground state, with the release of a single photon. In the case of ammonia, the excitation transition goes from state *X* to *C'* and the deexcitation transition from state *C'* to *A*. State *A* is predissociative and therefore not populated. The emission transition then has an upper state, *C'*, with a higher population then the lower state, A. This is called inverted population and forms the basis for all laser systems. In effect this inverted population along the beam path sets up a temporary laser cavity where lasing can occur. Through the spontaneous release of photons directed along the beam path a cascade of coherent photons are released. In short, a coherent laser beam along the same path as the original probe laser is created. This process is sometimes termed Amplified Spontaneous Emission (ASE) [10]. As the detector needs to be perpendicular to the beam in LIF measurements, all the photons released in the stimulated emission cascade correspond to a signal loss.

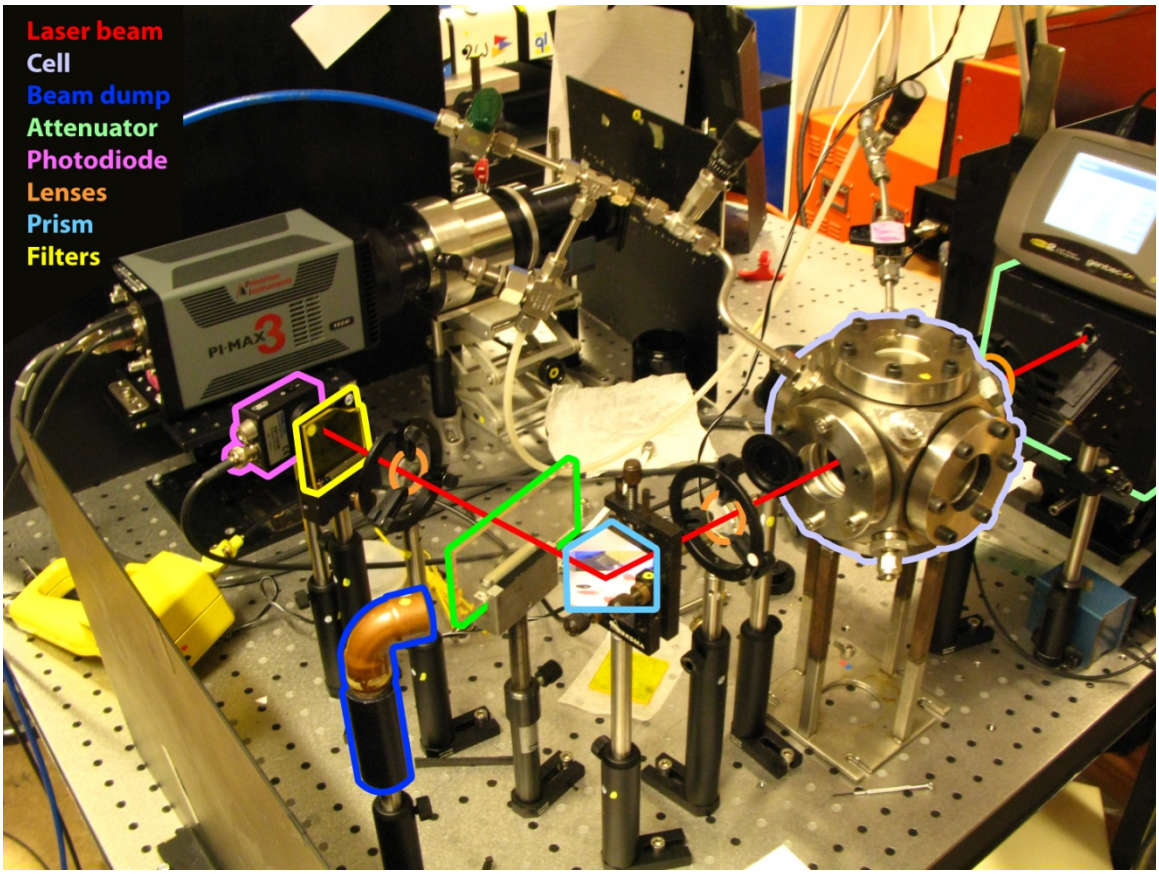

Figure 5-9: Image showing parts of the setup used for measuring the stimulated emission.

Determination of the behavior of stimulated emission from two-photon excitation of ammonia was carried out focusing the laser beam with a spherical lens (f=150 mm) in order to attain sufficient irradiance. The focus was in the centre of the same cell used in the power dependence measurements for the LIF signal. As the stimulated emission propagates along the same path as the laser beam itself it was necessary to use filtering to remove the light coming from the laser beam. This was achieved by using boron-silicate optics and filters downstream of the cell, to allow only the stimulated emission, it being at ~570 nm, to pass through to the detector. The remaining signal was collected on a photo-diode (DET 10A/M Thorlabs) using two spherical lenses, both with f=100 mm. The output from the photo-diode was sent to a digital oscilloscope (LeCroy Wavemaster) for acquisition and storage.

The strength of the stimulated emission depends on much the same parameters as the strength of the LIF signal. Power-, concentration- and pressure dependence has been determined. Of particular importance is that the stimulated emission did not reach detectable levels until the laser irradiance exceeded 10 GW/cm^2. This is an order of magnitude larger than the irradiance levels achieved in the power dependence measurements for the LIF signal, and larger still than the irradiance used in imaging. It is therefore assumed that stimulated emission does not significantly influence the LIF signal during planar LIF (PLIF) measurements. However, signal loss due to stimulated emission needs to be considered when attempting to detect low concentrations of ammonia in point measurements using a focused beam.

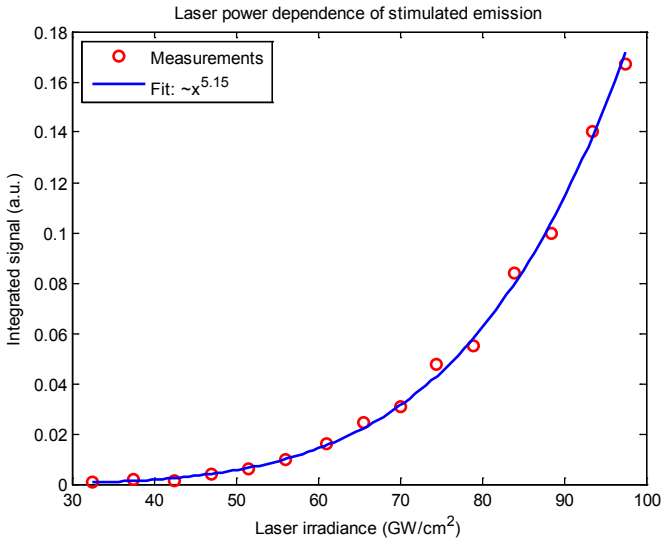

Figure 5-10: Power dependence of stimulated emission. The strength of the stimulated emission shows a very rapid growth with laser irradiance. For calculations of irradiance, the focused spot was determined to be approximately 50 µm in diameter. The emitted light from the stimulated emission was visible by eye.

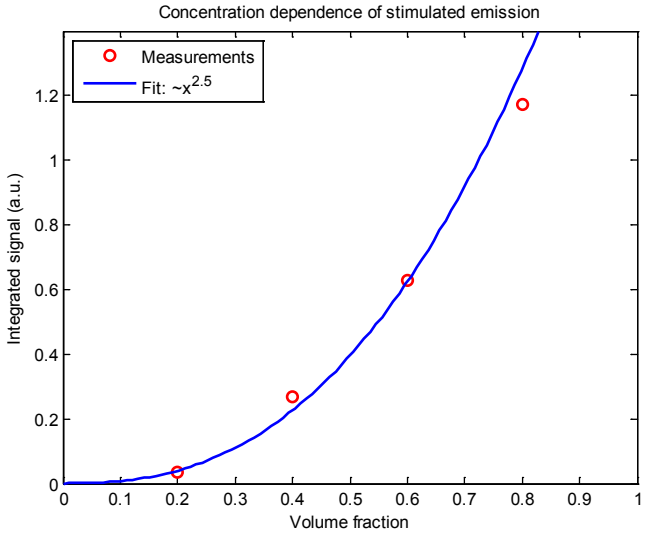

Figure 5-11: Concentration dependence of stimulated emission. As the number density of ammonia increases the strength of the stimulated emission increases rapidly.

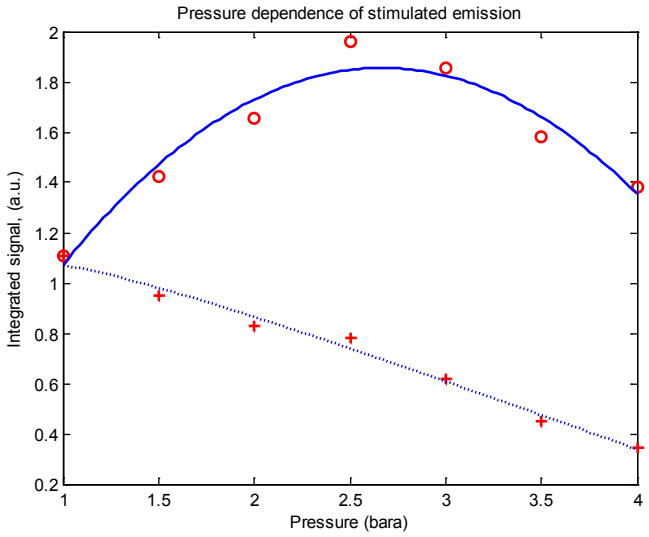

Figure 5-12: Pressure dependence of stimulated emission. The pressure broadening of the absorption feature and the emitted photon energy distribution results in a decrease of the stimulated emission with increasing pressures. The circles indicate the integrated stimulated emission signal, and the crosses are the same data with pressure normalization.

5.7 Images

In this section, images of ammonia using LIF are presented. Most of the images are done in flames as this is safer than flowing ammonia into the air. Flames also provide a convenient way of determining the capacity for the imaging technique to resolve concentration gradients as the flame has structure and form. Some cell measurements have also been done in cooperation with a team working with catalyst research.

5.7.1 Flame

The flame measurements were done using two different burners, both water-cooled. The first burner used had an opening of 10 mm and a long pre-mixing tube. The second burner used had a 2 mm opening and a sintered plug providing a co-flow around the flame. During the concentration dependence measurements (section 5.3), single-shot images were taken in order to evaluate the signal-to-noise ratio. The definition of signal-to-noise ratio used in this work is:

$$SNR = \frac{\mu}{\sigma}, \tag{IX}$$

where μ is the mean signal strength and σ is the standard deviation. 100 single-shot images were taken for each concentration level. The SNR was evaluated from an area of the images that showed strong, homogeneous signal. The area used is shown in Figure 5-10. SNR was then calculated for each image in the measurement series, and the resulting SNR for each concentration setting was taken as the average SNR for each individual image. SNR vs. ammonia concentration is shown in Figure 5-11. These results (together with further measurements at lower concentrations (paper pending)) indicate a lower detection limit with the current setup at approximately 800 ppm for single-shot images in turbulent flow.

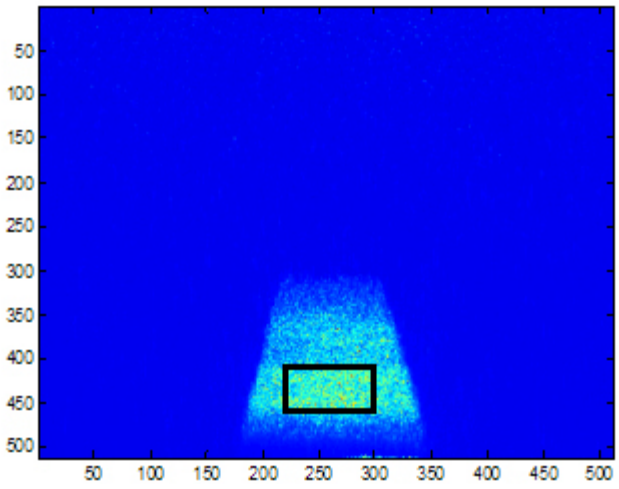

Figure 5-13: LIF image of pre-mixed flame. The fuel consisted of 10% ammonia, the rest was methane, giving an ammonia concentration of 10000 ppm of the total gas flow. The black rectangle indicates the area used for calculating the SNR.

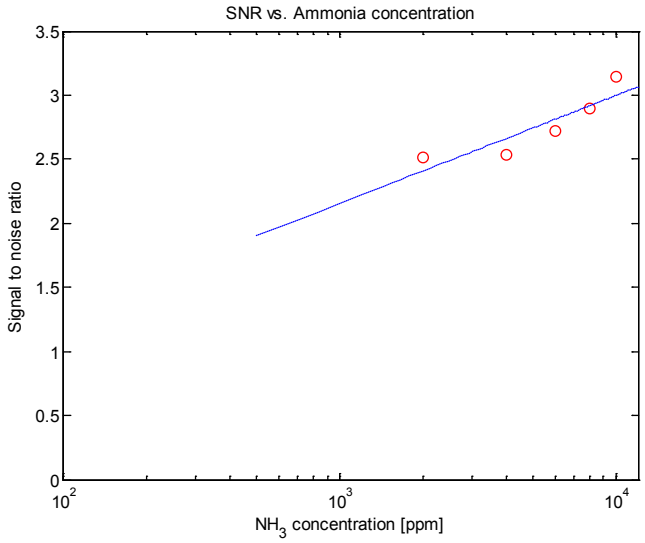

Figure 5-14: Calculated SNR vs. ammonia concentration. The dotted line shows a proposed extrapolation towards lower concentrations that fits with additional data (not shown here).

The following pages show images taken during these measurements with observations and explanations in the captions.

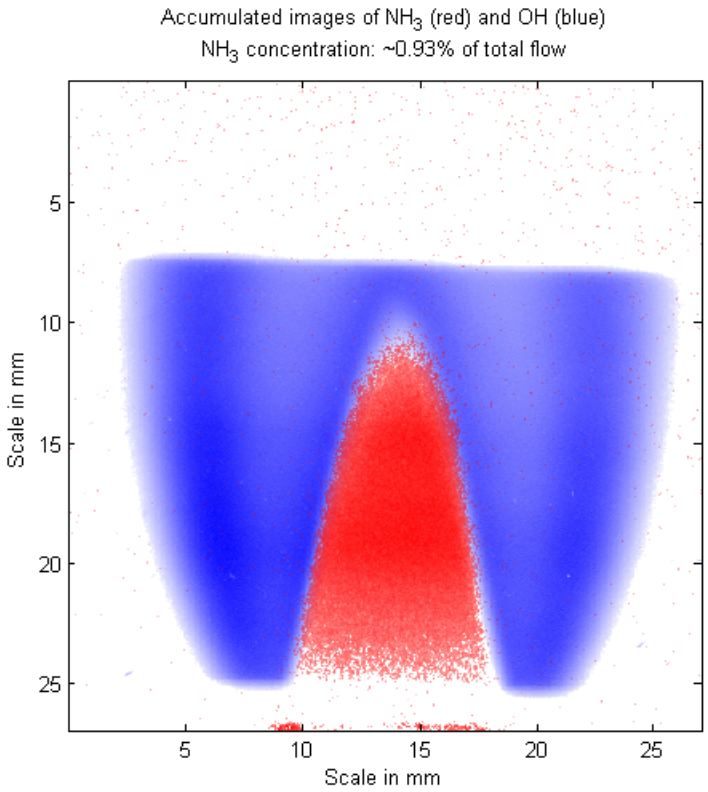

Figure 5-15: PLIF imaging of OH and NH_3 on a water-cooled Bunsen-type burner. The images consist of 100 accumulations. The excitation energy was 10mJ. Each single-shot image of ammonia had a SNR of approximately 2.

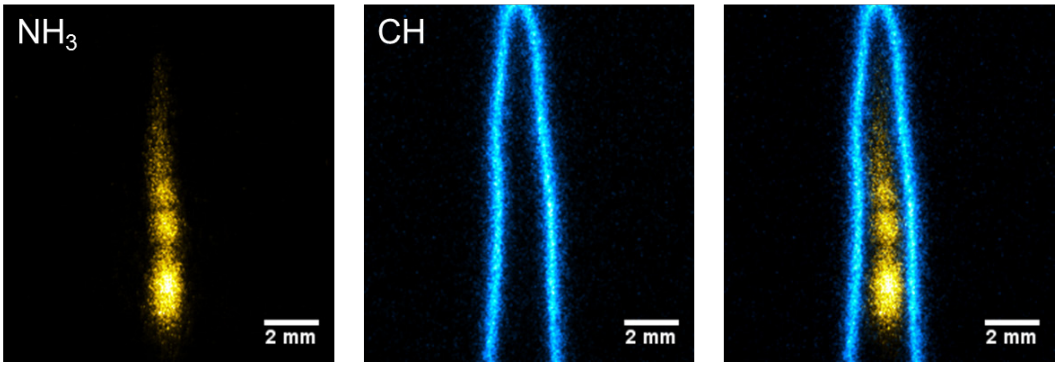

Figure 5-16: Simultaneous images of CH and NH_3 for a laminar flame. There is an observable gap between the cold flow cone in the central part where signal from NH_3 can be detected and the flame reaction zone. This indicates that ammonia decompose in the flame preheat zone.

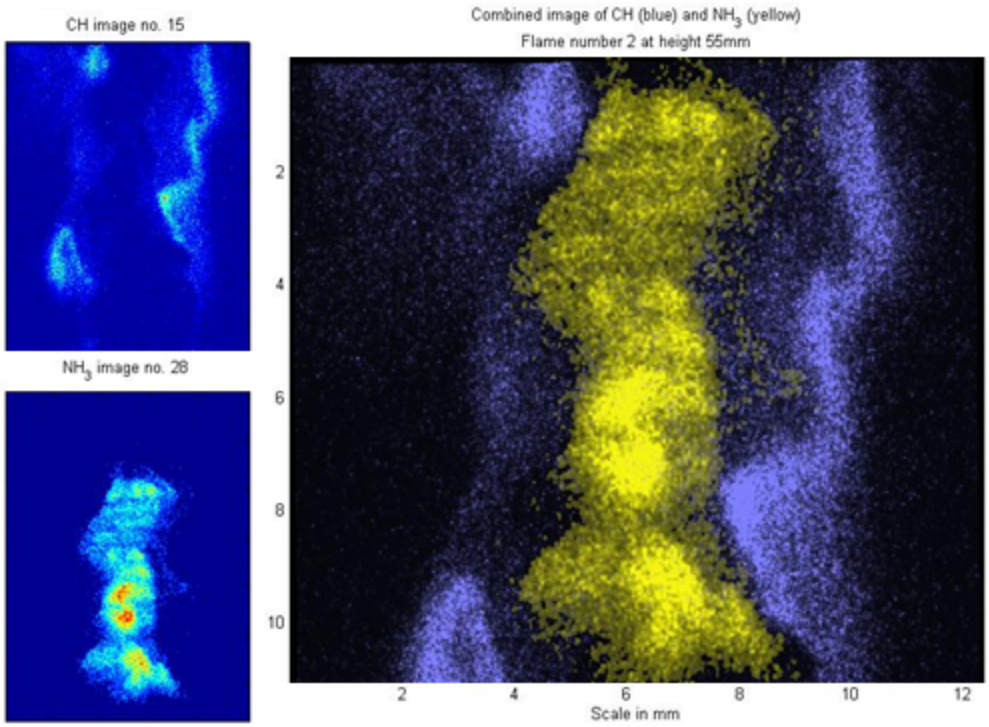

Figure 5-17: Simultaneous images of CH and NH_3 for a turbulent flame. The images are separated by ~100 ns and thus can be considered simultaneous as the flow features are static at such small timeframes. The images are taken using a 2 mm burner with a sintered plug around it providing a co-flow. The co-flow helped to stabilize the flame. The flow rate was set to 80 m/s and the stoichiometric ratio set at 1. 20% of the fuel was pure ammonia, the rest methane, meaning that the total flow consisted of 2.2% ammonia. As the concentration in this image is not homogenous, it is difficult to determine the SNR according to equation (IX). A measure to use is that the signal strength is more than 50 times that of the background variation. There is still some shot noise in the areas that fluoresce, but one cannot easily distinguish between noise and concentration variations in this region.

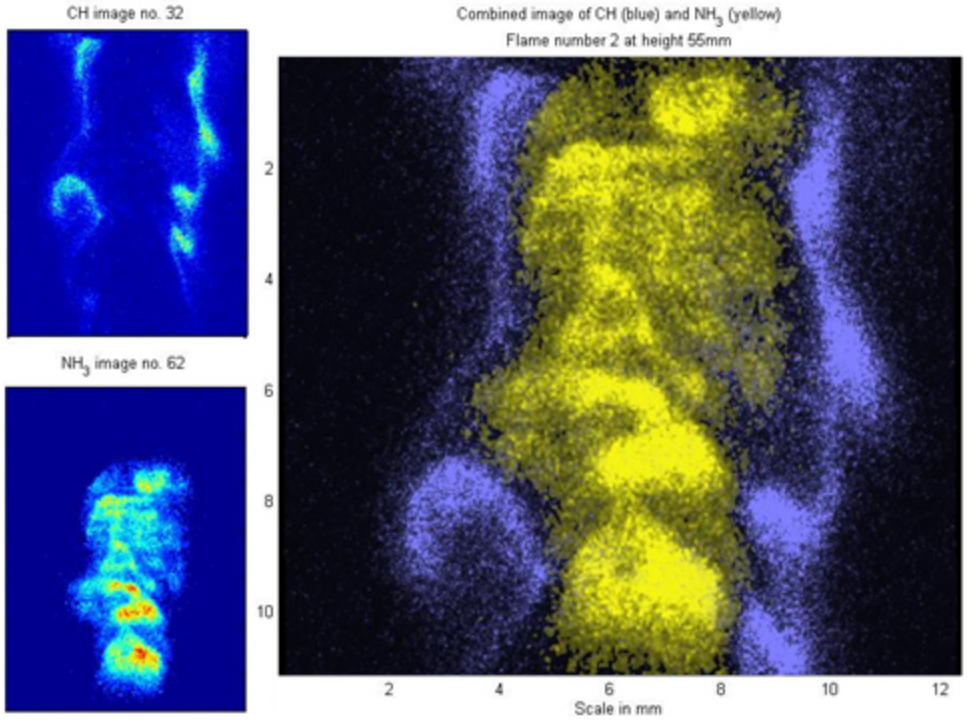

Figure 5-18: Simultaneous images of CH and NH_3. The flame conditions are the same as in Figure 5-17. Observe the complex flow-features in this image and the lack of overlap between the two signals. CH is a short lived radical that is created in the reaction zone of a flame. The blue signal in the figure could then be taken as indicating the position reaction zone of the flame. Observe that the ammonia signal does not extend into the reaction zone indicating that the ammonia is rapidly consumed in flame conditions. One can also observe that the strongest ammonia signal often corresponds to the weakest CH signal.

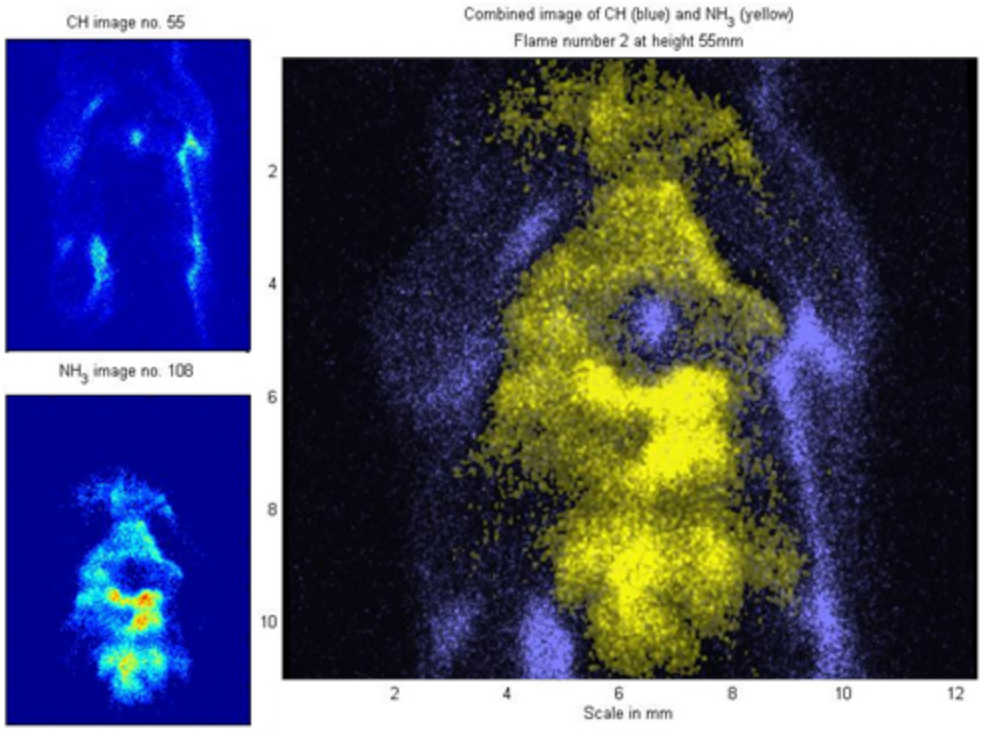

Figure 5-19: Simultaneous images of CH and NH_3. The flame conditions are the same as in Figure 5-17. In this image a small pocket or island of CH is nested within the ammonia signal. This again neatly demonstrates the exclusive behavior of the two species.

5.7.2 Measurements in cell

The cell measurements were done in cooperation with J. Zetterberg and S. Blomberg. These measurements utilized the LIF based technique to measure the concentration of ammonia directly above a small sample of catalytic material. Specifically, the effects of ammonia oxidation on the sample's surrounding gas were investigated. The sample could be heated and its temperature measured using an IR camera. The gas exiting the sample chamber was flowed through a mass spectrometer where the composition of the gas could be evaluated.

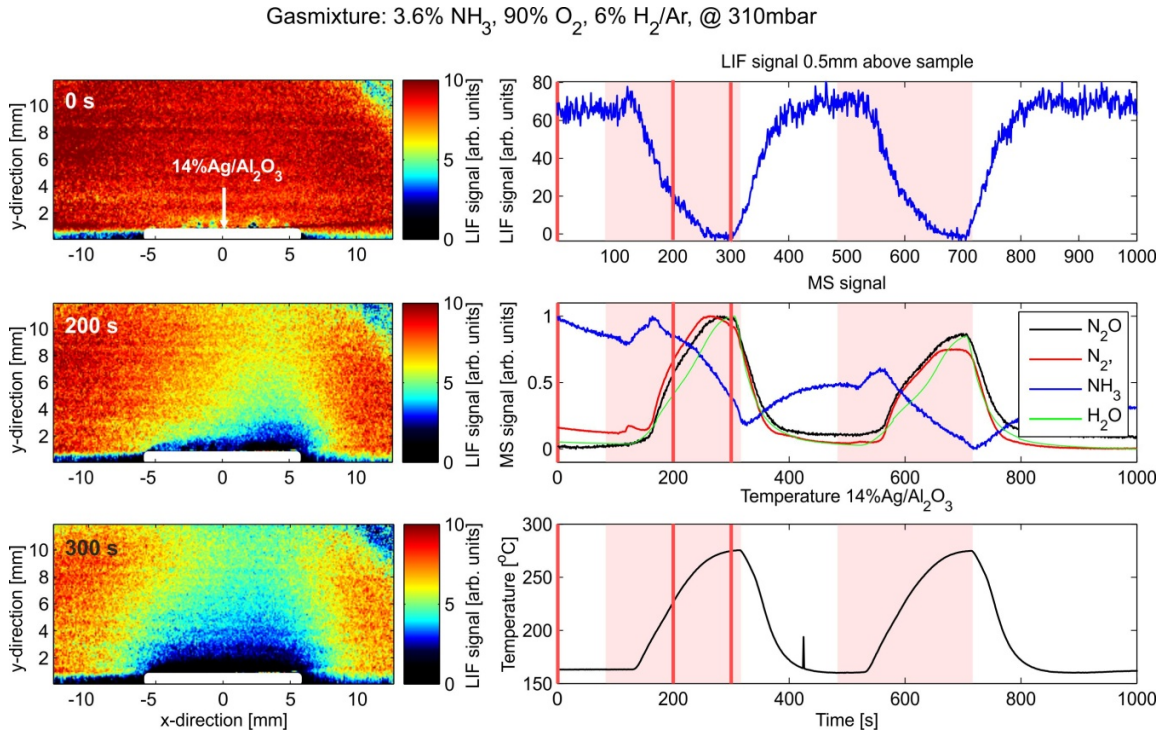

Figure 5-20: NH_3 PLIF measurements in cell containing ammonia reducing catalyst sample. During the experiment, H_2-gas was flushed into the flow passing through the cell at the times highlighted with pink in the right side plots. H_2 acts to drastically lower the activation temperature and efficiency of the sample and the flushing procedure thus gives a neat way of evaluating the sample behavior as it transitions between active and inactive. The left side shows 10-shot averaged images of the ammonia concentration above the sample for different times of the flush cycle. The images are adjusted for background and laser-profile. The vertical red lines on the plots to the right side indicate the times of the images.

The top right graph in the above figure shows the total LIF signal from an area approximately 1 mm above the surface of the sample. After switching from seeding argon to seeding hydrogen into the flow (indicated by the pink areas of the graph) the LIF signal rapidly declines after a small lag of some 50 seconds. This lag is probably due to the slow flow of gas through the sample cell so that it takes some time for the hydrogen to reach the critical concentration needed to activate the sample. Also note that the right part of the sample (see centre image left) is activated before the rest of the sample. In the images obtained from the IR camera mounted above the sample cell this was even clearer as here it could be seen that a very small area just at the edge of the right side of the sample got hot very rapidly. This indicates that this area was activated faster and earlier than the rest of the sample. A working hypothesis for why this happened is that this area consisted of a very thin ledge of catylic material jutting out from atop the bulk of the sample. This thin ledge had a larger active surface relative to its thickness than the rest of the sample and thus did not require as much energy to heat up.

When switching from seeding hydrogen and back to seeding argon the LIF signal rises rapidly to the same level it had before the hydrogen seeding. There is no noticeable lag this time as the declining hydrogen concentration simply makes the ammonia oxidation less efficient and no "deactivation" concentration is needed for this effect to be seen on the LIF signal. The relatively long time it takes before the sample is again inactive is again likely due to the slow exchange of gas in the call.

The middle right graph of Figure 5-15 shows some of the data obtained from the mass spectrometer. This data is currently not evaluated, nor is the shown graph properly normalized, but it does show qualitatively how the activation of the sample affects the composition of the gas flow

exiting the cell. It should be emphasized that the different species shown in the graph are on different scales. As the initial gas supplied into the cell contains no N_2O, N_2 nor H_2O it is assumed that the concentration of these species should be at, or close to, zero when the sample is inactive. The relative concentration of NH_3 should be stable in the initial conditions. The slight decline in NH_3 concentration during the first ~150 seconds is likely due to pressure variations within the system. Hopefully the effects of these pressure variations can be removed with proper normalization of the data.

After the switch from argon the hydrogen there again is a slight lag before anything happens with the sample. In this case there is however a slight increase in the concentration of NH_3 before it starts to decline. This slight increase coincides with the activation of the right edge of the sample and it is believed that the concentration change is due to a small pressure increase within the cell caused by the rising temperature. The lag between the supposed pressure increase caused by temperature and the change in gas composition is again thought to be due to the slow exchange of gas through the cell. A pressure change within the cell would influence the system almost directly, whereas a change in gas composition needs time to reach the mass spectrometer. Alternatively, the slight rise is due to the sample storing adsorbed NH_3 while inactive and releasing this stored gas as it heats up. This hypothesis is supported by the fact that there is no observed lag when switching from hydrogen seeding to argon seeding. The observed decrease of NH_3 coincides with the decrease of LIF signal as well as the increase of the concentrations of N_2O, N_2 or H_2O.

After switching back to argon again there is a rapid change in the composition of the gas mixture. Some of this rapid change could be attributed to pressure changes induced by the rapid cooling of the sample and its surrounding gas.

The lower right graph of Figure 5-15 shows the average temperature of the surface of the sample. Qualitatively it follows the LIF signal though inverted. The small spike just after the 400 second mark is due to a software glitch.

6 Conclusion and discussion

6.1 Viability of detection

This work has proven that 2-D LIF imaging of ammonia using two-photon excitation is viable for diagnostics. The governing parameters have been determined, and single-shot imaging has been successfully implemented. The lower limit of detection with the current equipment and setup is estimated to be 800 ppm for single-shot measurements. Narrower laser-sheets, or point-wise measurements, together with image accumulations are expected to push the detection limit down to the order of tens of ppm.

6.2 Limitations

The main limitation of the two-photon LIF is the relatively poor lower detection limit. The quadratic dependence on irradiance means that the width of the laser-sheets needs to be rather narrow in order for the signal to be strong enough. This limits the size of the imaging area to narrow bands along the laser path. A technical solution to this would be to allow the laser-sheet to sweep across the area of interest and in such a way image this area iteratively over several shots, each shot illuminating a different band of the final image. Another solution could be to use a multi-pass setup, where the laser beam is reflected back and forth in a zigzag pattern across the area of interest, facilitating single-shot images of larger areas. These solutions are, however, demanding to implement outside of laboratory conditions.

6.3 Further work

6.3.1 Investigation of PFLIF using excimer laser

Cross-sections for two-photon excitation has been found to be of the order of 10^{-50} cm^2 [28], whereas the single photon excitation of ammonia at 193.82 nm has a cross-section of 2×10^{-17} cm^2 [29]. The cross-section for the excitation of amidogen is not yet determined, but is assumed to be in the order of 10^{-20} cm^2. The combined cross-section for the two-step process of photo-dissociation of ammonia to the electronically excited NH (see section 3.2.2) would then be the product of each individual cross-section, due to the two processes being independent. This means that the expected cross-section for the PFLIF excitation process could be more than 10 orders of magnitude larger than the cross-section for the two-photon excitation process used in the experimental part of this thesis. It is then further expected that the detection limits would be much lower when using PFLIF than two-photon excitation LIF.

The use of PFLIF for ammonia detection has not been investigated before, and it could therefore prove a tremendous boon should the technique work as well as could be expected. Imaging of large-scale flow features as well as low concentrations could potentially be achievable.

6.3.2 Ammonia/urea coincidence measurements

The use of traces species is prevalent for purposes of mapping the flow of gas or mist that are injected into a flow. Determining the concentration distribution of ammonia near the surface of a catalyst could potentially be carried out using a tracer species as well. Tracer species are molecules that show very strong LIF signals even at low concentrations. A tracer species should follow the flow of the species that are to be investigated, i.e. the dissipation rate, evaporation rate and reaction rate of the tracer species needs to match that of the investigated species.

A proposed solution to track low concentrations of ammonia is to use a tracer species. The tracer species used would be tested by using simultaneous imaging of the tracer and ammonia to verify that they follow each other. Doing this under the pressures, temperatures and flow rates expected in an applied measurement should ensure that the tracer accurately indicates the ammonia distribution.

A further refinement of this technique would be to find a tracer species that not only follows gaseous ammonia, but that can be injected together with the urea, and then evaporate and dissipate so that it tracks the released ammonia. Investigating this would be done using the same principle as the ammonia/tracer coincidence measurements, but would be more difficult from a technical side. The reason for the added difficulty is that in order to accurately mimic the evaporation and hydrolyzation of urea to ammonia, a heated reactor with a mist-injection system would have to be used. Depending on the SCR-system that is to be investigated; there could even be the need for including a urea catalyst in order to ensure that the tracer follows the ammonia in a realistic manner.

6.3.3 Absorption measurements

As the absorption line that best suits absorption measurements has been identified herein, the next step would be to experimentally verify the line strengths and positions, and then to determine the lowest detection limits.

6.3.4 Photolytic catalysis

An investigation of the possibilities of utilizing photon-assisted SNCR has been suggested. SNCR (Selective Non-Catylic Reduction) is based on much the same chemistry as SCR, but no catalyst is involved in the reactions between ammonia and NO. The technique is only efficient in a narrow temperature window cantered at 1250 K. Below 1000 K the reaction is too slow and above 1500 K the increase of generated OH results in a net increase of NOx. Additionally, excess oxygen is required for the process to happen efficiently. The chemical reactions involved are not all known, though the available data suggest the reactions in the following diagram are involved [30]:

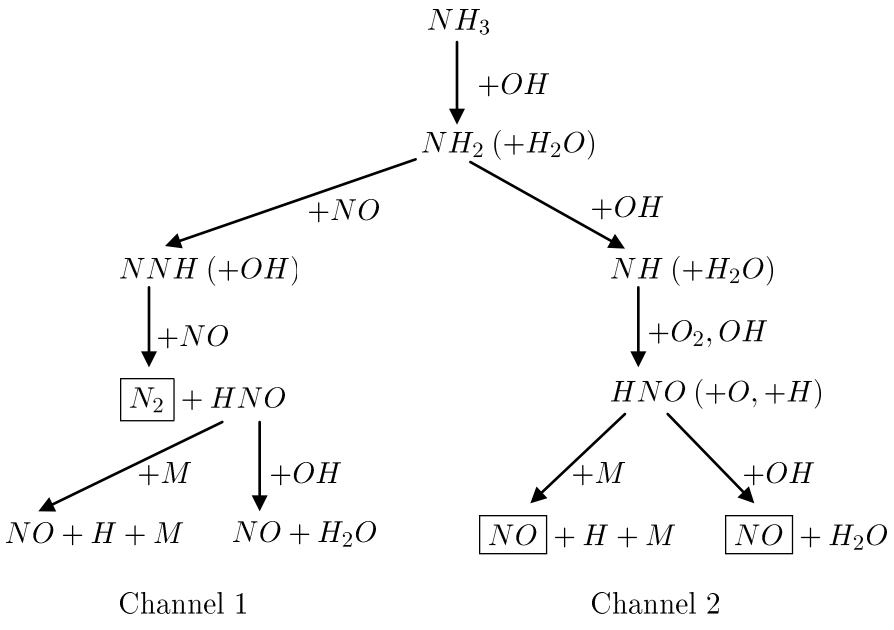

As is evident from the above diagram the reaction is dependent on OH in order to initiate. The initial step generates amidogen through the reaction between ammonia and OH. The amidogen then branches off into a two-step reaction where two NO molecules are reduced. The resulting product then reacts to form one molecule of NO; thus the process in channel 1 as a whole removes one NO molecule per amidogen molecule. Channel 2 results only in increasing the NO, and therefore this channel should be suppressed if possible. As this channel is dependent on OH it is clear that one way of suppressing it would be to minimize the OH available.

One possible way of achieving this is by removing the initial dependence on OH, and so removing the need for excess oxygen. As it is known that the excited states of ammonia are dissociative it is possible to initiate the reaction through photodissociation by illuminating the gas with UV-light. Ideally the light used should cover a narrow spectral range and be at a suitable wavelength so that the photons are preferentially absorbed by ammonia molecules. LEDs would be the preferred option due to their robustness and efficiency, but LEDs in the UV-range required are not yet commercially available. Nevertheless, the general principle is still valid and should be investigated to prepare for the technical development. LEDs with wavelengths around 210 nm have been operated under laboratory conditions, though these had a low efficiency [23]. It is reasonable to expect that these LEDs could soon become available, and light at ~210 nm would be near ideal for the photodissociation of ammonia. In this chapter calculations are based on a hypothetical system using SNCR initiated by UV-light.

In a flow of flue gas, ammonia is injected and allowed to dissipate. By passing through a section of piping illuminated by UV-light the SNCR reaction is initiated. The amount of power needed to dissociate ammonia in a flow can be calculated from the following equation:

$$P = Q\phi_{NH_3}\frac{hc}{\lambda}\frac{pN_A}{TR},$$

where Q [m^3 s^{-1}] is the volume flow rate, ϕ_{NH_3} [-] the ammonia volume concentration, h [J s] is Planck's constant, c [m s^{-1}] is the speed of light, λ [m] the photon wavelength, p [Pa] the pressure, T [K] the temperature, N_A [mol^{-1}] Avogadro's number and R [m^3 Pa K^{-1} mol^{-1}] the gas constant. In this simplified equation it is assumed that every photon is absorbed by an ammonia molecule that subsequently dissociates. In addition, the equation does not consider the efficiency of the light emitter. Below is an example of calculated power consumption for such a system:

Table 6-1: Assumed parameters for calculation of expected power consumption

Flow:	$Q = 0.1\,m^3/s$
Ammonia concentration:	$\phi_{NH_3} = 500\,ppm$
Temperature:	$T = 1000\,K$
Pressure:	$p = 10^5\,Pa$
Photon wavelength:	$\lambda = 208.7\,nm$
Power required to dissociate the ammonia:	$\mathbf{P = 345\,W}$

The wavelength 208.7 nm has been chosen above because ammonia has a relatively large absorption cross-section at this wavelength [29], and it is reasonably close to the reported 210 nm limit for LEDs. The flow rate is an approximation of the flow rate from a large engine.

An alternate approach to this is to use a photochemical reactor to dissociate the ammonia prior to injection into the flue gas flow. It has been found that this approach can lower the temperature required for SNCR to occur to 600°C [31]. The benefit of this approach is that the size and cost of the system can be kept at a minimum. Unfortunately no experiments using urea-based ammonia carriers as the source of the injected ammonia have yet been carried out. It has been found that the ideal photon flux is such that each mole of ammonia absorbs a bit more than N_A photons [31]. This makes it possible to predict the expected power consumption of an activated ammonia injection system.

$$A = 1 - e^{-\alpha N d}$$

$$N_p = A\frac{\lambda}{hc}\frac{PRT}{Q\phi_{NH_3}p} \approx N_A$$

$$P \approx \frac{N_A}{A}\frac{Q\phi_{NH_3}p}{RT}\frac{hc}{\lambda},$$

where N [cm^{-3}] is the number of ammonia molecules per unit volume, A [-] is the absorptivity of ammonia, α [cm^2] is the absorption cross-section of ammonia at λ, d [cm] is the distance of the photon path, and N_p [mol^{-1}] is the number of absorbed photons per mole of ammonia.

Below is an example calculation of the power consumption for such a system:

Table 6-2: Assumed additional parameters to those presented in Table 6-1

Absorption cross-section:	$\alpha = 8.11 \times 10^{-18}\, cm^2$
Distance of photon path:	$d = 10\, cm$
Power required to dissociate the ammonia:	$\mathbf{P \approx 775\ W}$

Increasing the distance of the photon path will decrease the power requirement, though the unit would require more space. At a path length of 50 cm, the power required is down to 364 W, but a further increase in path length does not yield any significant reduction in power consumption as the absorptivity approaches unity.

An important aspect to note is that the temperature in these calculations is higher than the temperatures usually found in the typical SCR environment. However, as SNCR is not dependent on a catalyst, the injection point for the activated ammonia can be placed nearer the engine. The increased temperatures are required for the SNCR-reactions to progress at high enough rates.

7 Acknowledgements

First and foremost I would like to thank my supervisor Zhongshan Li for his support and help during the work with this thesis. Christian Brackmann Ph. D. was a big help during the experimental stages of the work and gave me valuable and instructive lessons in practical laboratory work, as well as helping me with the analysis of the data from the measurements. I hope our paper gets accepted! I am grateful for the technical input from Henrik Birgersson Ph. D., Senior Engineer at Scania CV AB, who was my corporate supervisor. My visits to Södertälje were instructive and interesting. I would also like to thank Scania CV AB for financial support during my work. Carl-Erik Magnusson, course administrator, provided valuable input for how the thesis should look. I thank Bo Zhou for his help in the laboratory during the later stages of measurements. A special thanks to Johan Zetterberg and Sara Blomberg for letting me test the measurement technique on their test rig during our measurement campaign. Finally, I would like to thank the love of my life, Malin Österman, for always being there for me and supporting me.

8 Bibliography

1. NIOSH. *Documentation for Immediately Dangerous To Life or Health Concentrations (IDLHs): Ammonia*. 1994 may 1994 [cited 2013 14 jan.]; Available from: http://www.cdc.gov/niosh/idlh/7664417.html.
2. Science Stuff, I. *Material Safety Data Sheet*. 2006 [cited 2013 14 jan.]; Available from: http://www.sciencestuff.com/msds/C1191.html.
3. Registry, A.f.T.S.a.D. *Toxicologial Profile for Ammonia*. 2004 [cited 2013 14 jan.]; Available from: http://www.atsdr.cdc.gov/tfacts126.pdf.
4. Georgiev, N. and M. Alden, *Two-dimensional imaging of flame species using two-photon laser-induced fluorescence.* Applied Spectroscopy, 1997. **51**(8): p. 1229-1237.
5. Duncan, A.B.F., *The ultraviolet absorption spectrum of ammonia.* Physical Review, 1935. **47**(11): p. 0822-0827.
6. Herzberg, G., *Rydberg Spectra of Triatomic Hydrogen and of the Ammonium Radical.* Faraday Discussions, 1981. **71**: p. 165-+.
7. Ashfold, M.N.R., et al., *Fluorescence Excitation and Emission-Spectroscopy of the C'1a1' Rydberg State of Ammonia - Assignment of the Schuster Bands of Ammonia.* Journal of Molecular Spectroscopy, 1986. **117**(2): p. 216-227.
8. Koebel, M., M. Elsener, and M. Kleemann, *Urea-SCR: a promising technique to reduce NOx emissions from automotive diesel engines.* Catalysis Today, 2000. **59**(3-4): p. 335-345.
9. Fang, H.L. and H.F.M. DaCosta, *Urea thermolsis and NOx reduction with and without SCR catalysts.* Applied Catalysis B-Environmental, 2003. **46**(1): p. 17-34.
10. Eckbreth, A.C., *Laser Diagnostics for Combustion Temperature and Species*. Second ed. Combustion Science and Technology Book Series, ed. W.A. Sirignano1996, The Netherlands: Gordon and Breach Publishers. 596.
11. Gislason, E.A., N.H. Sabeli, and J.W. Wood, *New Form of the Time-Energy Uncertainty Relation.* Physical Review A, 1985. **31**(4): p. 2078-2081.
12. Ehn, A., *Towards Quantitative Diagnostics using Short-Pulse Laser Techniques*, in *Division of Combustion Physics*2012, Lund University: Lund, Sweden. p. 118.
13. Westblom, U. and M. Alden, *Laser-Induced Fluorescence Detection Of NH3 In Flames With The Use Of 2-Photon Excitation.* Applied Spectroscopy, 1990. **44**(5): p. 881-886.
14. Franck, J., *Elementary processes of photochemical reactions.* Transactions of the Faraday Society, 1926. **21**(3): p. 0536-0542.
15. Condon, E., *A theory of intensity distribution in band systems.* Physical Review, 1926. **28**(6): p. 1182-1201.
16. Kenner, R.D., et al., *2-Photon Formation of NH/ND(A3-Pi) in the 193 nm Photolysis of Ammonia .1. Mechanism Andidentification of the Intermediate Species.* Chemical Physics, 1987. **118**(1): p. 141-152.
17. Donnelly, V.M., A.P. Baronavski, and J.R. Mcdonald, *Arf-Laser Photo-Dissociation of NH3 at 193-nm - Internal Energy-Distributions in NH2x2b1 and A2a1, and 2-Photon Generation of NH-A3-Pi and B1-Sigma+.* Chemical Physics, 1979. **43**(2): p. 271-281.
18. Kenner, R.D., F. Rohrer, and F. Stuhl, *Generation of NH(A1delta) in the 193 Nm Photolysis of Ammonia.* Journal of Chemical Physics, 1987. **86**(4): p. 2036-2043.
19. Donnelly, V.M., A.P. Baronavski, and J.R. Mcdonald, *Excited-State Dynamics and Bimolecular Quenching Processes for NH2(A2a1).* Chemical Physics, 1979. **43**(2): p. 283-293.
20. Kenner, R.D., R.K. Browarzik, and F. Stuhl, *2-Photon Formation of NH/ND(a 3ii) in the 193 nm Photolysis of Ammonia .2. Photolysis of NH2.* Chemical Physics, 1988. **121**(3): p. 457-471.
21. Georgiev, N. and M. Alden, *Developments of laser-induced fluorescence for two-dimensional multi-species imaging in flames.* Spectrochimica Acta Part B-Atomic Spectroscopy, 1997. **52**(8): p. 1105-1112.
22. Hole, O.M., *In situ HF-concentration measurements in combustion environments using diode-laser absorption spectroscopy*, in *Department for Combustion Physics* 2011, University of Lund: Lund. p. 51.
23. Taniyasu, Y. and M. Kasu, *Surface 210 nm light emission from an AlN p-n junction light-emitting diode enhanced by A-plane growth orientation.* Applied Physics Letters, 2010. **96**(22).

24. Mihalcea, R.M., et al., *Diode-laser absorption measurements of CO2, H2O, N2O, and NH3 near 2.0 mu m.* Applied Physics B-Lasers and Optics, 1998. **67**(3): p. 283-288.
25. Webber, M.E., D.S. Baer, and R.K. Hanson, *Ammonia monitoring near 1.5 mu m with diode-laser absorption sensors.* Applied Optics, 2001. **40**(12): p. 2031-2042.
26. Western, C.M., *PGOPHER, a Program for Simulating Rotational Structure*, 2010, University of Bristol.
27. Nolde, M., K.M. Weitzel, and C.M. Western, *The resonance enhanced multiphoton ionisation spectroscopy of ammonia isotopomers NH3, NH2D, NHD2 and ND3.* Physical Chemistry Chemical Physics, 2005. **7**(7): p. 1527-1532.
28. Glownia, J.H., et al., *The Mpi Spectrum of Expansion-Cooled Ammonia - Photophysics and New Assignments of Electronic Excited-States.* Journal of Chemical Physics, 1980. **73**(9): p. 4296-4309.
29. Cheng, B.M., et al., *Absorption cross sections of NH3, NH2D, NHD2, and ND3 in the spectral range 140-220 nm and implications for planetary isotopic fractionation.* Astrophysical Journal, 2006. **647**(2): p. 1535-1542.
30. Miller, J.A., M.C. Branch, and R.J. Kee, *A Chemical Kinetic-Model for the Selective Reduction of Nitric-Oxide by Ammonia.* Combustion and Flame, 1981. **43**(1): p. 81-98.
31. Kambara, S., et al., *Removal of nitric oxide by activated ammonia generated by vacuum ultraviolet radiation.* Fuel, 2012. **94**(1): p. 274-279.
32. Rothman, L.S., et al., *The HITRAN 2008 molecular spectroscopic database.* Journal of Quantitative Spectroscopy & Radiative Transfer, 2009. **110**(9-10): p. 533-572.
33. Olivero, J.J. and R.L. Longbothum, *Empirical Fits to Voigt Line-Width - Brief Review.* Journal of Quantitative Spectroscopy & Radiative Transfer, 1977. **17**(2): p. 233-236.
34. Whiting, E.E., *An Empirical Approximation to Voigt Profile.* Journal of Quantitative Spectroscopy & Radiative Transfer, 1968. **8**(6)

Appendix A

Below left is shown the temperature stability of the most suitable lines identified. The line strength data were collected from the HITRAN database (see [32] for documentation) and evaluated using JavaHAWKs and MATLAB. Following the temperature stability graph are nine graphs showing the spectrum in the immediate vicinity of each line. Overlaid each ammonia spectrum is the spectra of water and CO_2 in order to check for species overlap. The water and CO2 are set to ratios corresponding to complete stoichiometric methane/air combustion. The simulated spectra were made using a Voigt-profile approximation [33, 34] and accounts for self-broadening and air-broadening effects.

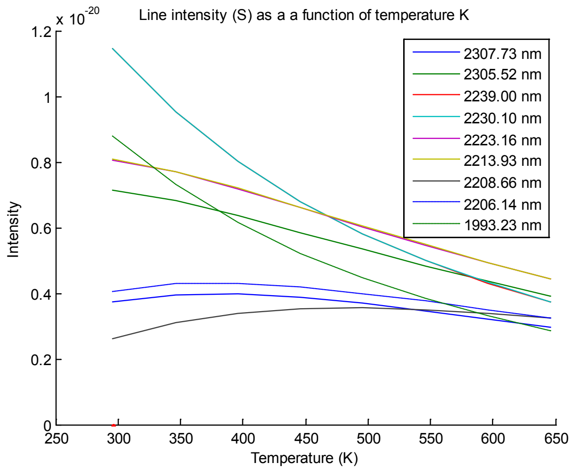

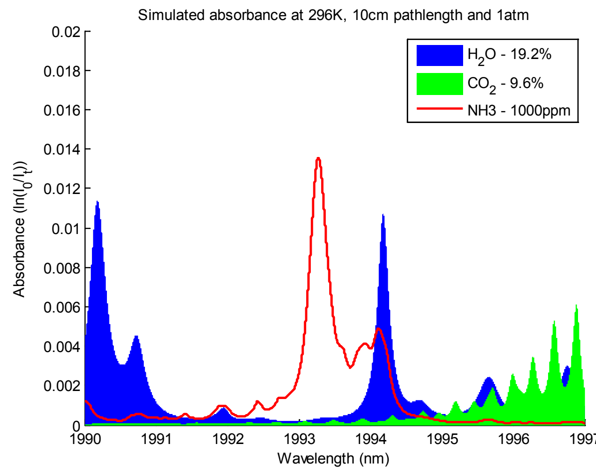

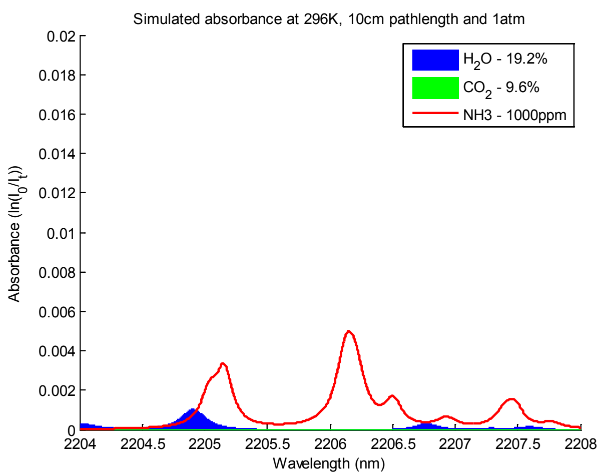

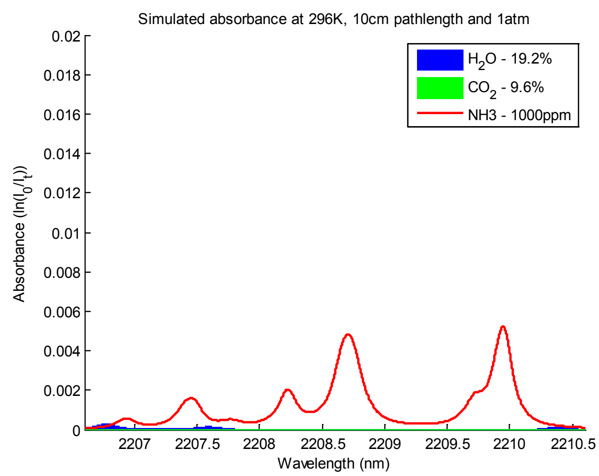

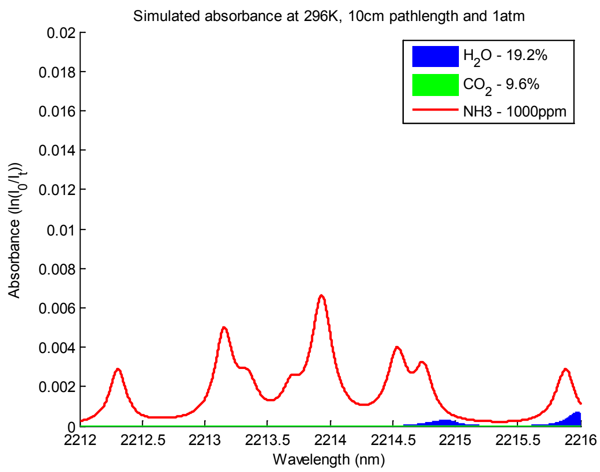
Simulated absorbance at 296K, 10cm pathlength and 1atm
H_2O - 19.2%
CO_2 - 9.6%
NH3 - 1000ppm
Absorbance ($ln(I_0/I_t)$)
Wavelength (nm)
0 0.002 0.004 0.006 0.008 0.01 0.012 0.014 0.016 0.018 0.02
2212 2212.5 2213 2213.5 2214 2214.5 2215 2215.5 2216

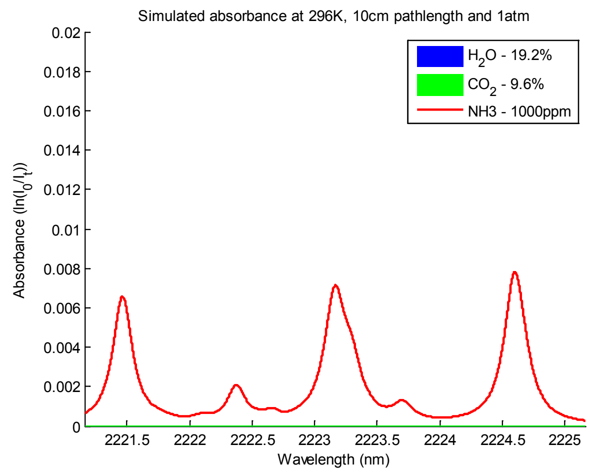
Simulated absorbance at 296K, 10cm pathlength and 1atm
H_2O - 19.2%
CO_2 - 9.6%
NH3 - 1000ppm
Absorbance ($ln(I_0/I_t)$)
Wavelength (nm)
0 0.002 0.004 0.006 0.008 0.01 0.012 0.014 0.016 0.018 0.02
2221.5 2222 2222.5 2223 2223.5 2224 2224.5 2225

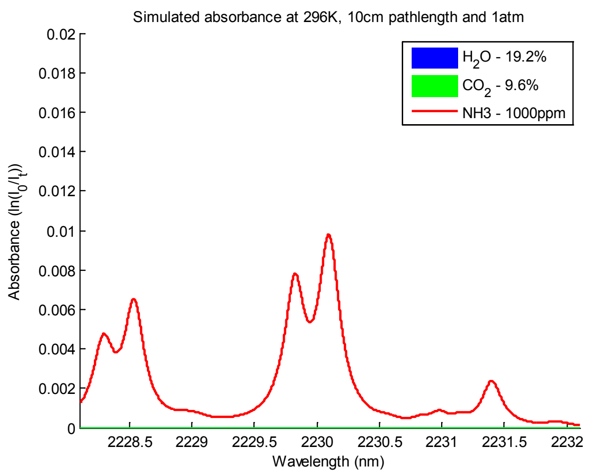
Simulated absorbance at 296K, 10cm pathlength and 1atm
H_2O - 19.2%
CO_2 - 9.6%
NH3 - 1000ppm
Absorbance ($ln(I_0/I_t)$)
Wavelength (nm)
0 0.002 0.004 0.006 0.008 0.01 0.012 0.014 0.016 0.018 0.02
2228.5 2229 2229.5 2230 2230.5 2231 2231.5 2232

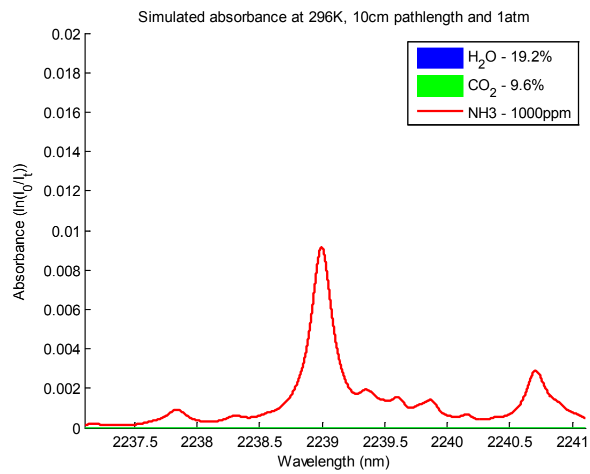
Simulated absorbance at 296K, 10cm pathlength and 1atm
H_2O - 19.2%
CO_2 - 9.6%
NH3 - 1000ppm
Absorbance ($ln(I_0/I_t)$)
Wavelength (nm)
0 0.002 0.004 0.006 0.008 0.01 0.012 0.014 0.016 0.018 0.02
2237.5 2238 2238.5 2239 2239.5 2240 2240.5 2241

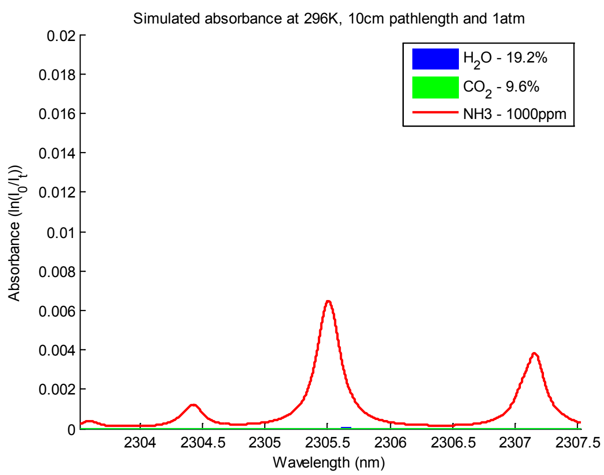
Simulated absorbance at 296K, 10cm pathlength and 1atm
H_2O - 19.2%
CO_2 - 9.6%
NH3 - 1000ppm
Absorbance ($ln(I_0/I_t)$)
Wavelength (nm)
0 0.002 0.004 0.006 0.008 0.01 0.012 0.014 0.016 0.018 0.02
2304 2304.5 2305 2305.5 2306 2306.5 2307 2307.5

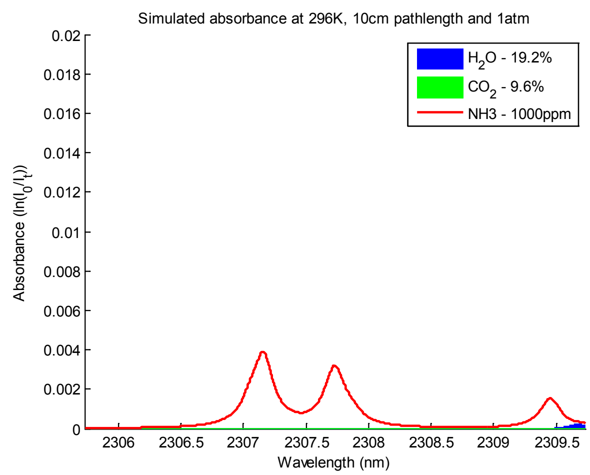
Simulated absorbance at 296K, 10cm pathlength and 1atm
H_2O - 19.2%
CO_2 - 9.6%
NH3 - 1000ppm
Absorbance ($ln(I_0/I_t)$)
Wavelength (nm)
0 0.002 0.004 0.006 0.008 0.01 0.012 0.014 0.016 0.018 0.02
2306 2306.5 2307 2307.5 2308 2308.5 2309 2309.5